Universidad de Concepción

The formation of compact dwarf ellipticals through merging star clusters

(Formación de enanas elípticas compactas por medio de la fusión de cúmulos globulares)

Tesis para ser presentada en la dirección de postgrado de la Universidad de Concepción para optar al grado de

Magister en ciencias con mención en física

Fernanda Cecilia Urrutia Zapata

Asesor: Dr. Michael Fellhauer

Concepción, Chile

Marzo 2018

Agradecimientos

Me gustaría agradecer a todas las personas que me apoyaron durante estos años de estudios. A mis compañeros y amigos con los que nos dimos fuerzas y ánimo para seguir adelante y terminar esta importante etapa.

También a mi familia, a mi mamá, Norma Zapata, mi hermana, Francisca Urrutia y mi padre, Sergio Urrutia. Ya que sin ellos no habría logrado nada de lo logrado academicamente ni en la vida.

Doy gracias a mis profesores que me enseñaron e instruyeron con paciencia durante todos mis años universitarios. En especial a mi profesor tutor Michaell Fellhauer que me impulsó e insentivó a avanzar cada vez más en mi desarrollo como cientifica. Además a los miembros del Theory and Star Formation Group en Concepción por la buena disposición a aconsejar y de responder todas las dudas que surgían durante mi trabajo en esta tesis.

Por último agradecer a Dominik Schleicher y a el programa basal por la ayuda financiera en este proceso, a la Universidad de Concepción y a Dirección de Postgrado por lo mismo ya que fue muy útil para asistir a escuelas y congresos para aprender de otros temas y exponer acerca de este trabajo en otros centros de investigación.

Abstract

In the last decades, extended old stellar clusters have been observed. They are like globular clusters (GCs) but with larger sizes (a limit of effective radius (R_{eff}) of 10 pc is currently seen as reasonable). These extended objects (EOs) cover a huge range of mass. Objects at the low mass end with masses comparable to normal globular clusters are called extended clusters or faint fuzzies (Larsen & Brodie (2000)) and objects at the high-mass end are called ultra compact dwarf galaxies (UCDs). Ultra compact dwarf galaxies are compact object with luminositys above the brigtest known GCs. UCDs are more compact than typical dwarf galaxies but with comparable luminosities. Usually, a lower mass limit of 2 $\times 10^6$ $M_\odot$ applied.

Fellhauer & Kroupa (2002a,b) demostrated that object like ECs, FFs and UCDs can be the remnants of the merger of star clusters complexes, this scenario is called the Merging Star Cluster Scenario. A more concise study was performed by Brüns et al. (2009, 2011).

Our work tries to explain the formation of compact elliptical(cE). These objects are a comparatively rare class of spheroidal galaxies, possessing very small R_{eff} and high central surface brightnesses (Faber 1973). cEs have the same parameters as extended objects but they are slightly larger than 100 pc and the luminosities are in the range of -11 to -12 Mag.

The standard formation scenario of these systems proposes a galaxy origin. cEs are the result of tidal stripping and truncation of nucleated larger systems. Or they could be a natural extension of the class of elliptical galaxies to lower luminosities and smaller sizes.

We want to propose a completely new formation scenario for cEs. In our project we try to model cEs in a similar way that UCDs using the merging star cluster scenario extended to much higher masses and sizes. We think that in the early Universe we might have produced sufficiently strong star bursts to form cluster complexes which merge into cEs. So far it is observationally unknown if cEs are dark matter dominated objects. If our scenario is true, then they would be dark matter free very extended and massive "star clusters".

Resumen

En las últimas décadas, viejos cumulos estelares extendidos han sido observados. Son como, cúumulos globulares (GCs) pero con tamaños más grandes (un limite de R_{eff}=10 pc es actualmente considerado razonable). Estos objetos extendidos (EOs) cubren un gran rango de masas. Objetos que se posicionan en el extremo inferior de este rango con masas comparables con cúmulos globulares normales, son llamados extended clusters (EC) o faint fuzzies (FFs) (Larsen & Brodie (2000)) y objetos en el extremo superior son llamados ultra compact dwarf galaxies (UCDs). Ultra compact dwarf galaxies son objetos compactos con luminosidades más grandes que las de los GCs más brillantes conocidos. UCDs son más compactos que las típicas galaxias enanas pero con luminosidades comparables a ellas. Usualmente, se aplica un límite inferior de masa de 10^6 $M_\odot$.

Fellhauer & Kroupa (2002a,b) demostraron que objetos como ECs, FFs and UCDs pueden ser remantentes de la fusión de complejos de cúmulos estelares, este escenario es llamado Merging Star Cluster Scenario. Un estudio más consiso fue hecho por Brüns et al. (2009, 2011).

Nuestro trabajo trata de explicar la formación de compact elliptical(cE). Estos objetos son una clase comparativamente rara de galaxias esferoidales, poseyendo un muy pequeo R_{eff} y un muy alto brillo superficial central (Faber 1973). cEs tienen los mismos parámetros que los objetos extendidos pero son un poco más grandes que 100 pc y tienen luminosidades en el rango de -11 y -12 Mag.

El escenario de formación estándar de estos sistemas propone un origen galáctico. cEs son el resultado de la remoción de marea y la luego truncación de grandes sistemas con nucleos. O ellos pueden ser la extensión natural de las galaxias elípticas a más pequeñas luminosidades y tamaños.

Queremos proponer un escenario completamente nuevo de formación de cEs. En nuestro proyecto tratamos de modelar cEs de una forma muy similar a la formación de UCDs, usando el merging star cluster scenario pero ahora con masas y tamaños mucho más grandes. Pensamos que en el universo temprano podríamos haber producido star bursts lo suficientemente fuertes para formar un complejo de cúmulos que se fusionaron en cEs. Hasta ahora es observacionalmente desconocido si las cEs son dominadas por materia oscura. Si nuestro escenario es verdadero, entonces las cEs seran extendidos, libres de materia oscura y "cumulos globulares" muy masivos.

Contents

List of Figures

List of Tables

Chapter 1

Introduction

Our work tries to explain the formation of compact elliptical (cE). These objects are a comparatively rare class of spheroidal galaxies, possessing very small effective radius ($R_{\rm eff}$) defined as the projected radius that enclosed half of the total luminosity of one object. The central surface brightnesses is high, compared to dwarf ellipticals of the same size (Faber 1973). One of the most important characteristic of cE is the high stellar density due the high surface brightness and the small $R_{\rm eff}$.

The prototype galaxy for this types of galaxy is the 32nd object in the catalog of Messier (1850), called M32, which is a satellite ofAndromeda galaxy (M31). M32 (Fig 1.1)has an $R_{\rm eff}$ of the bulge of 27" (∼100 pc), a effective surface brightness in the bulge of 18.23 R-mag arcsec^{-}2(Graham 2002) and a velocity dispersion of 76 ± 10 km/s (van der Marel et al. 1998).

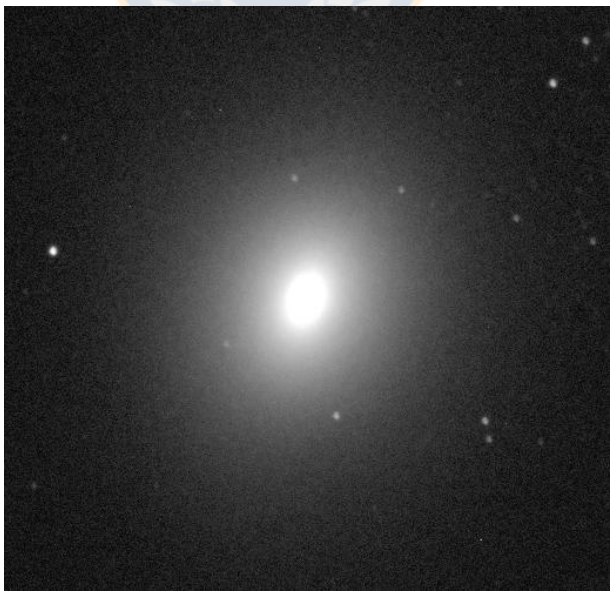

Figure 1.1: Messier 32, the prototype galaxy for cEs galaxies. Image taken from Bill Keel's image collection at the University of Alabama.

The standard formation scenario of these systems proposes a galaxy origin. CEs are the result of tidal stripping and truncation of nucleated larger systems(Faber 1973). Or they could be a natural extension of the class of elliptical galaxies to lower luminosities and smaller sizes(Wirth & Gallagher 1984;Kormendy et al. 2009).

We want to propose a completely new formation scenario for cEs. In our project we try to model cEs in a similar way like Ultra Compact Dwarf galaxies (UCDs) in Brüns et al 2011, which are object with characteristics very similar to cE-high surface brightness, small $R_{\rm eff}$ so high stellar density- using the merging star cluster scenario extended to much higher masses and sizes (as you can see in figure 1.2). We think that in the Early Universe we might have produced sufficiently strong star bursts to form cluster complexes (groups of young massive stars clusters) which merge into cEs. So far it is observationally unknown if cEs are dark matter dominated objects. If our scenario is true, then they would be dark matter free very extended and massive "star clusters".

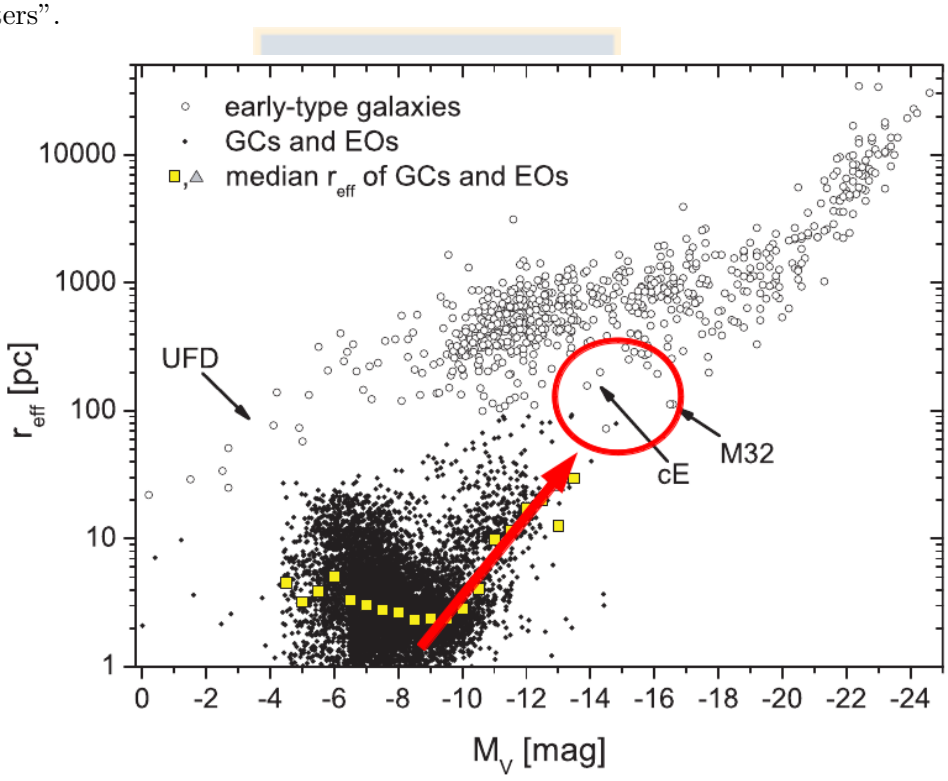

Figure 1.2: Size-luminosity diagram of spheroidal systems. Globular clusters, extended objects and UCDs are shown as black dots. Open circles denote spherical systems regarded as galaxies (from right to left) from normal ellipticals via dwarf ellipticals to dwarf spheroidals. The part of parameter space inhabited by cEs is circled red. The arrow denotes the direction from which our models try to explain the formation of cEs. Image taken from Brüns 2013 PhD thesis, University of Bonn.

1.1 Globular Clusters

Globular clusters (SCs) are groups of 100.000 to 1.000.000 old stars which are gravitationally bound(William 1991), masses between 10^4 to 10^6 $M_\odot$, with magnitudes between -5 to -10 and median effective radii of 3 pc(Brüns 2013 PhD thesis, University of Bonn).
The stars in a SC formed at the same time. The distribution of the stars in the globular cluster is close to spherical with a high density in the centre(Talpur,J (1997)).
Globular clusters have a high density of stars from 0.4 stars per cubic parsec in the outer parts of the SC to 100 or 1000 stars per cubic parsec in the center of the cluster(Talpur (1997).
Globular clusters are typically orbiting galaxies. A lot of them are found in the halo of galaxies. There are at least 150 known clusters in the Milky Way, but bigger galaxies like M31 should have at least 500 SCs(P. Barmby, J.P. Huchra 2001), or M87 that have 13,000 (Harris 1996 Globular Cluster Systems list, McMaster University)
If we talk about the formation of these systems they are formed in regions rich in gas and interstellar dust called molecular clouds. Also, there is no example of a known SC with dark matter.

1.2 Extended object - From faint Fuzzies to Ultra Compact Dwarf Galaxies

In the last years, extended and old stellar clusters have been observed, with a large mass range. Extended objects with masses comparable to normal globular clusters are called extended clusters (ECs) and objects with high masses are called ultra compact dwarf galaxies. In the middle we have other systems like Faint Fuzzies (FF).
Fig 1.3 shows the effective radius with the total V-band luminosity of 835 extended objects, of the catalog of Brüns 2013 PhD thesis, University of Bonn, in early-type and late-type galaxies.

The position of the extended clusters and ultra compact dwarf galaxies (UCDs) are labeled in the graphic.
Most of the objects are found in the magnitude range of about $M_V = -5$ to -13 mag. At $M_V =$ -8.5 mag the number of objects is much smaller than at lower and higher luminosities. A clear trend between the luminosity and the upper size limit is observed; the higher the luminosity,the larger the upper size limit.

Extended clusters are metal-poor clusters, they are like globular clusters but with larger sizes, there is not a physical size demarcation between SCs and ECs but an effective radius of 10 pc is seen as a reasonable limit (van den Bergh & Mackey 2004).

Fig 1.4 shows the effective radius against Galactic distance of SCs and ECs in the Milky Way in black, the Sag dSph in green, the LMC, the SMC and the Fornax dSph in red. Fig 1.5

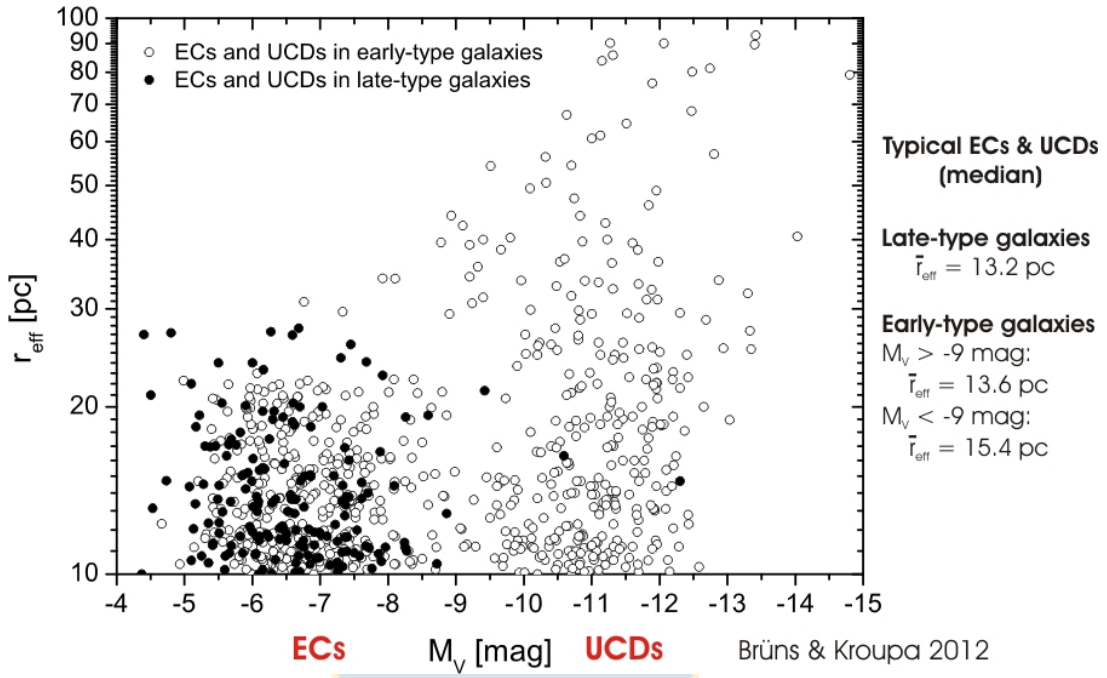

Figure 1.3: Luminosity(M_v)-size diagram. EOs in early-type galaxies are represented by open circles, and EOs in late-type galaxies, by black circles. Image taked by Brüns & Kroupa 2012.

shows the effective radius against the luminosity of SCs and ECs Milky Way in black, the Sag dSph in green, the LMC, the SMC and the Fornax dSph in red. In figure (1.4) and (1.5) the line at $r_{\rm eff} = 10$ pc indicate the separation between SCs and ECs.

We see Fig 1.4 ECs have positions in the outer part of the galaxy. If we consider all SCs of the Milky Way (SCs and ECs), the median Galactic distance is about 5 kpc, but if we only consider the ECs we have a median galactic distance of 72 kpc.

In Fig 1.5 we see that the ECs of the Milky Way are in general fainter than M_V = -7 mag. The median value is -5.7 mag, and the median luminosity of the entire SC sample is -7.2 mag. It is easy to see that most of the SCs are compact considering that the median effective radius of the 156 Milky Way clusters is 3.0 pc.

The most extended EC of the Milky Way is Palomar14 with effective radius of 27 pc.

Larsen & Brodie (2000) discovered several extended star clusters co-rotating with the disk of lenticular galaxy NGC1023, as Fig 1.6 shows. In this picture the black line marks the orientation of the galaxy, and the black circles are at a different distance to the center of the galaxy i.e 2, 4, 6, 8, 10 and 12 kpc. The gray box marks the image that Larsen & Brodie (2000) used to

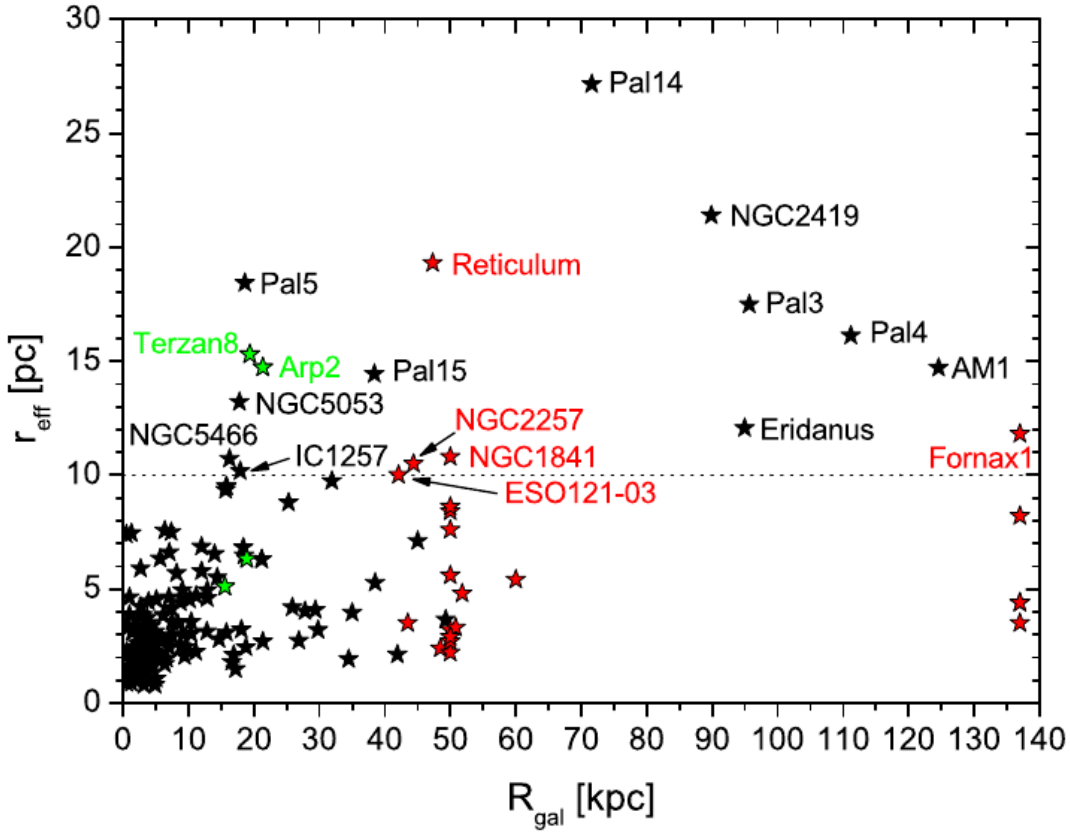

Figure 1.4: Effective radius with Galactic distance of SC and EC of the Mily Way in black the Sag dSph in green and the LMC the SMC and the Fornax dSph in red The line indicate the separation between SCs and ECs. Image taked by Brüns 2013 PhD thesis, University of Bonn.

detect Faint Fuzzy(FF). The green crosses mark the confirmed FF, and the white crosses are the remaining candidates from Larsen & Brodie (2000).

This objects were discovered when they observed the galaxy and found a bimodal color distribution, they were called Faint Fuzzy (FF) due to their faint and extended appearance. The blue SCs of the sample in the NGC1023 are metal-poor having effective radius in average about 2.0 pc. The red SCs are metal-rich and the average radius is about 1.7 pc. (West et al. 2004) The sizes for the blue clusters are smaller than 7 pc, but the red clusters reach a size of 18 pc. Objects larger than 7 pc are generally fainter than the red compact objects. Larsen & Brodie (2000) studied the position of the faint object of NGC1023 and found that they are associated with the disk of the galaxy.

When Brodie & Larsen (2002) performed spectroscopic observations of the SC in NGC1023 they found that FFs show sign of co-rotation with the disk of the galaxy, but the compact red object didn't show this behavior, so they concluded that the FFs are a separate population

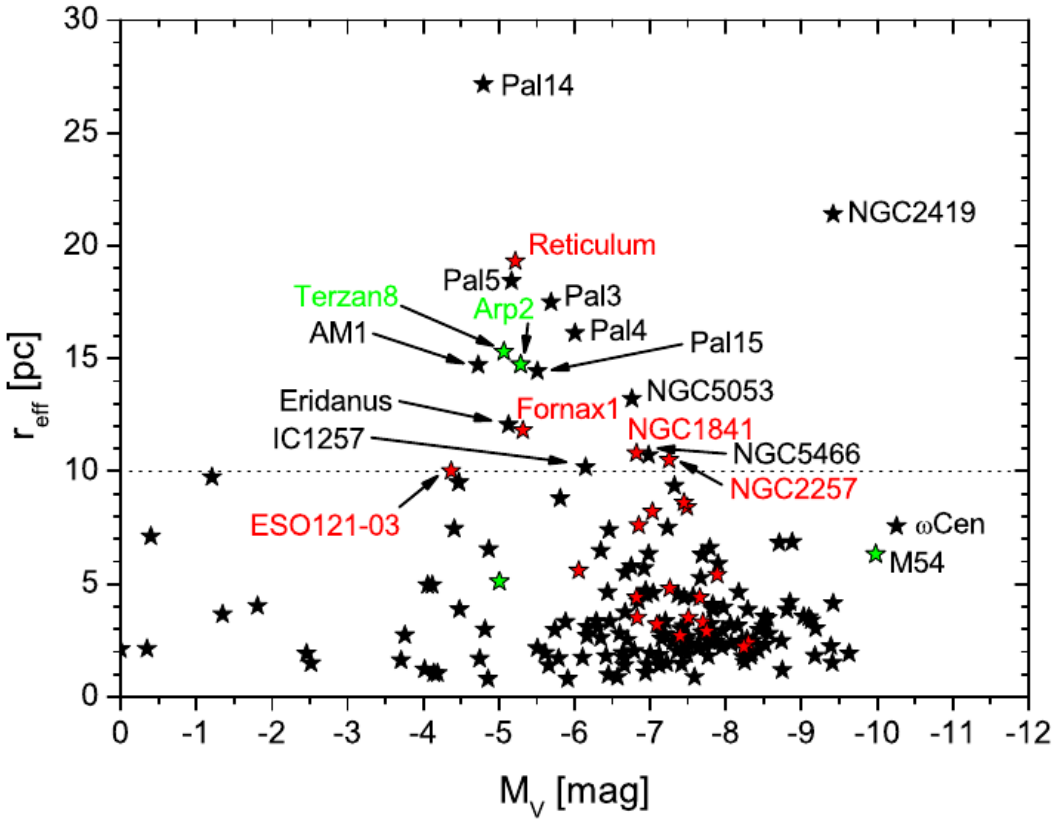

Figure 1.5: Effective radius with luminosity of Star clusters(SC) and Extended clusters(EC) of the Milky Way in black, the Sag dSph in green and the LMC, the SMC and the Fornax dSph in red. The line indicates the separation between SCs and ECs. Image taked by Brüns 2013 PhD thesis, University of Bonn.

associated with the disk.

FFs are often difficult to identified because they have quite similar structural parameters as halo ECs. The effective radius of FFs ranges from 7 pc to 13.4 pc and the median radius is 10.7 pc The luminosity range of the FFs that Larsen & Brodie (2000) found was from 21.4 mag to 25 mag.

To estimate the age of these objects they averaged all FF spectra to obtain a high signal to noise ratio. The age that they found seems to be older than 7-8 Gyr.
Then Burkert et al. (2005) analyzed the distribution and radial velocities of the FFs in NGC1023 and said that FFs are remnants of a past gravitational interaction forming a structure like a ring.

Today this types of galactic systems have also observed in other galaxies, like for example

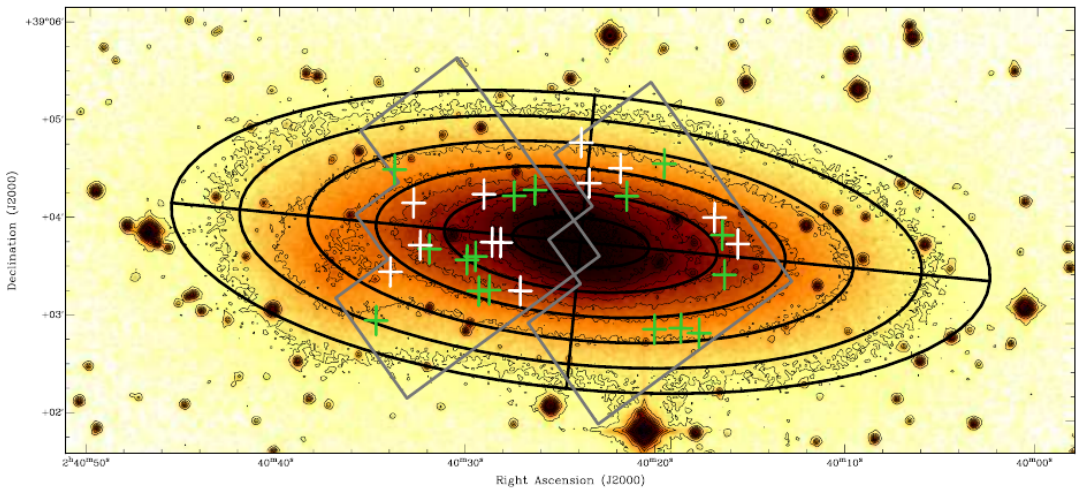

Figure 1.6: Digitized Sky Survey (DDS) image of the galaxy NGC 1023.The black line marks the orientation of the galaxy, and the black circles are at a different distance to the center of the galaxy i.e 2, 4, 6, 8, 10 and 12 kpc. The gray box marks the image that Larsen & Brodie (2000) use to detect FF. The green crosses mark the confirmed FF, and the white crosses are the remaining candidates from Larsen & Bodie (2000).

the lenticular galaxy NGC 1380 (Chies-Santos et al. 2007). And also even in other types of galaxies like the dwarf irregular galaxy NGC5195 (Lee et al. 2005)

Ultra compact dwarf galaxies are extended objects with high mass. They were discovered in the Fornax cluster by Hilker et al (1999) and Drinkwater et al.(2000). The principal characteristics of these systems are: Their luminosities are above the brightest known SCs and the effective radius of them is between 10 and 100 pc. So they are larger, brighter and more massive than SCs but more compact than typical dwarf galaxies of comparable luminosity. As the object in Fig 1.2 are part of a continuum there is not a clear division between the objects, but observers apply a lower mass limit of 2×10^6 $M_\odot$ (e.g. Mieske et al. 2008).

Fig 1.7 is a representative image of the size of a UCD compared to the Milky way.

The most extended UCD is VUCD7 discovered in the outer halo of the elliptical galaxy M87 of the Virgo cluster. It has a mass of 8.8×10^7 $M_\odot$(Evstigneeva et al. 2007) and an effective radius of 93.2 pc(Evstigneeva et al. 2008). The interpretation of the nature of these objects is controversial because of its parameters. The effective radius and total luminosity place them between the parameters of SC and dwarf galaxies.

Because of the controversial nature of these objects Kissler-Patig (2004) proposed the name ultra-diffuse star cluster consider this object more like a SCs. Then in 2005 Hasegan et al.

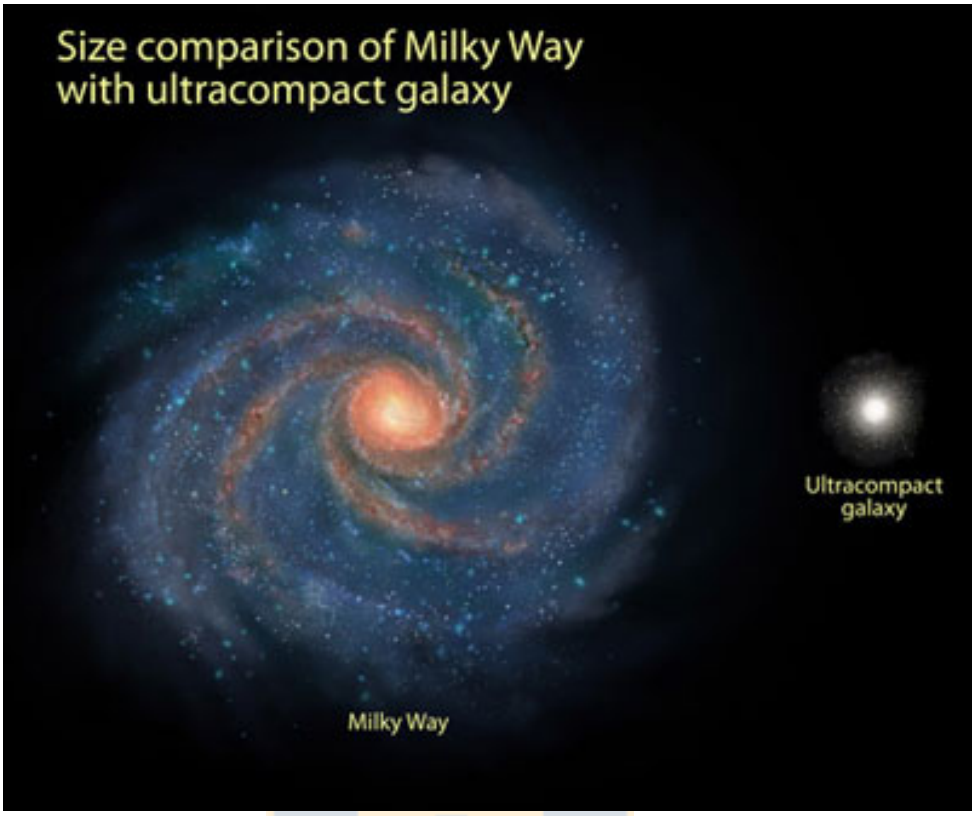

Figure 1.7: This is a representative image of the size of a UCD compared to the Milky way. Credit: NASA, ESA, A. Feild (STScI) and P. van Dokkum (Yale).

proposed the name dwarf-globular transition object.

Fig 1.8 shows a size-luminosity diagram. The position of SCs, ECs/FFs, and UCDs is labeled. Dashed lines denote lines of constant surface density and also the 'avoidance zone'(Hwang et al 2011) is shown, where in 2013 Forbes et al. found objects around the early-type galaxies NGC4278, NGC4649 and NGC4697. These objects are shown as blue and red symbols (corresponding to a division in color (g–z) = 1.1, equivalent to metallicity [Fe/H] = -1). It is clear that the largest and more luminous objects are blue, and on the opposite side of the diagram the objects with low luminosities are red.

If we talk about the age of this type of objects most of them have ages larger than 8 Gyr but there are also samples of young UCDs and with medium ages.
An example of a young version of UCD was discovered by Maraston et al 2004; a massive star cluster (W3) with an age between 300 and 500 Myr in the galaxy NGC7252. W3 has a mass of about 8×10^7 $M_\odot$ and an effective radius of 17.5 pc.
An example of a intermediate ages of 3.4 Gyr was found in the galaxy NGC4546 by Norris &

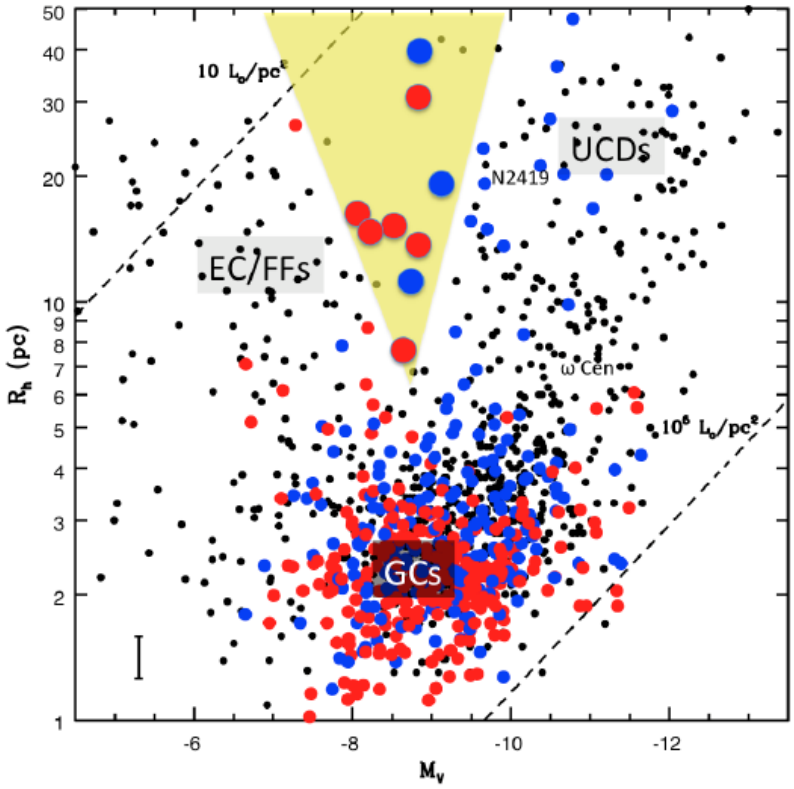

Figure 1.8: Size-luminosity diagram. Circles blue and red corresponding to a division at color (gz) = 1.1, equivalent to metallicity [Fe/H] = -1. The position of SCs, ECs/FFs, and UCDs is labeled. Dashed lines denote lines of constant surface density and also the avoidance zone (Hwang et al 2011) is shown with the objects found by Forbes et al (2013). Image taken from Forbes et al 2013.

Kannappan (2011). This UCD has a mass of 3×10^7 $M_\odot$ and an effective radius of 25.5 pc.

Also for several years astronomers have been debating about the formation scenario of these objects, and it is still a huge topic of discussion. Mainly the scenarios of formation can be subdivided into scenarios with a galaxy origin and scenarios with a star cluster origin.

Scenario with a SCs origin are where UCDs are the natural massive end of the distribution of SCs (Mieske et al. 2002) or where the UCDs are the result of the merger of SCs in a Cluster Complex (CC) (Fellhauer & Kroupa 2002b,a), this is called the Merging Star Cluster Scenario.(see section 1.5)

An example of a scenario without star cluster origin is the galaxy threshing scenario, in this scenario a nucleated dwarf interact with larger galaxies (typically early-type galaxies). The interaction of the dwarf galaxies and the bigger galaxy result in the loss of almost all stars of the main body except for the nucleus (Bekki et al. 2001). There are also people that claim that UCDs are remnants of primordial compact galaxies (Drinkwater et al. 2004).

1.3 Compact elliptical

Compact ellipticals (cE) have the same parameters as extended objects but they have R_{eff} in the range of 100 to 1000 pc and a mass between 10^8 and 10^{10} $M_\odot$ (Anna Ferré-Mateu et al. 2017). They are galaxies at the low-mass end of the elliptical sequence. The prototype is the Local Group dwarf galaxy M32(Huxor et al 2013). They are a very rare class of galaxies. They have very small effective radii and high central surface brightnesses (Faber 1973), as shown in figure 1.9 which is a size-luminosity diagram where SCs and EOs are plotted as black circles and the early-type galaxies are shown as open circles. The median effective radius per luminosity bin is given as yellow squares. The position that compact ellipticals take in this graphic is labeled with their prototype example M32. Also the position of ultra faint dwarf galaxies (UFD) found in the Milky Way is labeled as UFD.

Compact ellipticals are usually not isolated in the field, they are close to massive galaxies in groups or clusters but there are examples of isolated cE, like cE0 (CSCG 063-062) (Huxor et al 2013).
Until a few years ago the numbers of this types of galaxies identified until a distance of 100 Mpc was only a few dozen but in the last years this number has increase considerably(e.g Ferre-Mateu et al. 2017, Janz et al.2016 and references therein)

If we talk about the formation of these systems, many believe that they have a galactic origin and end in this system due to an interactions with a giant neighbor which leads to the tidal stripping and truncation scenario (Faber 1973).
Similar to the galaxy threshing scenario, in where nucleated dwarfs interact with larger galaxies (typically early-type galaxies). The interaction of the dwarf galaxies and the bigger galaxy result in losing almost all stars of the main body except for the nucleus (Bekki et al. 2001).

This scenario of stripping may have an origin either as a elliptical galaxy truncated with a dense core (e.g King 1962; Faber 1973) or be a bulge of a partially stripped disk galaxy (e.g Bekki et al. 2001)

Also, cEs have been considered as systems with an intrinsic origin due the natural extension of the class of elliptical galaxies to smaller sizes and lower luminosities (Wirth & Gallagher 1984; Kormendy et al. 2009).

Kormendy & Bender (2012) argue against the stripping scenario as: “not all cEs are companions of massive galaxies; many dSph galaxies are companions to massive galaxies yet are not truncated; bulges also sit at the compact end of the scaling relations for elliptical galaxies but are not truncated; and that unlike globular clusters, the object for ideas of tidal truncation, the dark matter halo of a dwarf galaxy will quickly lead to a merger with its massive host.”

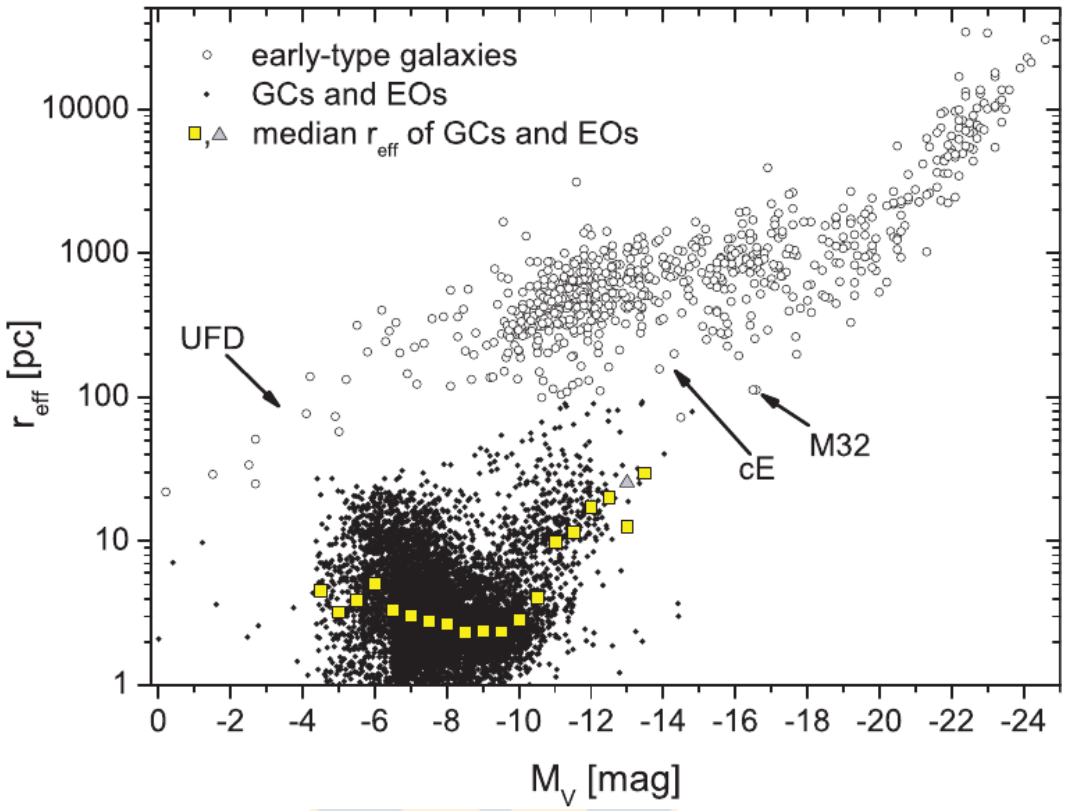

Figure 1.9: Size Luminosity diagram. SC and EOs are plotted as black circles and the early-type galaxies are shown as open circles. The median effective radius per luminosity bin is given as squares.
The position that compact ellipticals take in this graphic is labeled with their prototype example M32. Also the position of ultra faint dwarf galaxy (UFD) found in the Milky Way is labeled. The grey triangle shows the median effective radius, when the 6 exceptionally bright compact SCs with luminosities between $M_V = -12.5$ and $M_v = -14.5$ and an effective radius below 4 pc were removed in the bin at $M_V = 13.0$ mag. Image taken by Brüns 2013 PhD thesis, University of Bonn

Huxor et al. 2011 report two cEs, which show evidence of formation resulting from the ongoing tidal stripping of more massive progenitors (were the tidal tails are clearly visible) but then Huxor et al 2013 found the first isolated cE. Its isolated position suggests that stripping may not be the only scenario but there has to be an alternative channel to the stripping scenario for the formation of compact ellipticals.

1.4 Cluster complex (CC)

The Cluster Complexs contain from a few to hundreds of young massive stars clusters (YMCs). The size of those systems is in the range of a few hundred to ∼1 kpc in diameter. The mass of a CC is the sum of the mass of the YMSCs that it contains.

Observations show that most CCs have a massive concentration of star clusters in their centers and few to even hundreds of isolated stars clusters in their vicinity.(Bastian et al. 2005)

The formation of this CCs takes place in different enviroments for example, in Fig 1.10 the Antennae galaxies(NGC4038 + NGC4039) are shown. These are interacting galaxies leading to the formation of many CCs. The system is constituted by two spiral galaxies at a distance of approx 20 Mpc.
This two galaxies are colliding and because of that they are going trough a phase of a star burst. This strong interaction of stars and gas in this system leads to the formation of Young Massive Star Clusters(YMSCs).

The CCs in the Antennae are called knots. For example Knot S is the second brightest knot in this system, with a total luminosity of $M_V = -15.8$ mag (Whitmore et al. (1999)) and a $R_{\rm eff}$ of 155 pc. In the Fig 1.10.b the black circle is the radius of 450 pc that Whitmore et al. (1999) used to derive the total luminosity and the blue circle is the $R_{\rm eff}$ of Knot S.

The age of knot S is about 7 Myr (Whitmore et al. 1999), this involves a mass-to-light ratio of $log_{10}(M/L_V) = -1.6$ (Bruzual & Charlot 2003).

This low mass-to-light ratio leads to a total mass of knot S of 4.5×10^6 $M_\odot$. The white circle in figure 1.10.b is an object with 1/3 of the total mass in the center of the knot S (the size of this object is 18 pc (Bastian et al. 2013). Surrounding that central object, there are 94 objects, of which 33 are brighter than MV = -9 mag or more massive than 3.8×10^3 $M_\odot$ (Whitmore et al. 2010).

In Fig 1.11 it is possible to see the formation of a CC in a spiral galaxy. This formation takes place during an interaction with a small companion galaxy (Whirlpool galaxy M51). M51 is a grand-design spiral galaxy and has a neighbor galaxy called NGC5195. Bastian et al. (2005) found 11 CCs in the disk of M51 connected to the spiral arms of the disk, with ages younger than 10 Myr, with sizes between 85 and 240 pc, which cover a mass range of 0.3–3 $\times 10^5$ $M_\odot$. You can see an example of this in the zoom of one arm.

A clear example of formation in tidal tails is visible in the Tadpole galaxy (Fig 1.12). The blow-up picture shows the biggest (with effective radius of 160 pc) and most luminous CC in the tail (total luminosity of -14.45 mag(Tran et al 2003)). They demonstrated that the CC forms within the tidal tail at a the projected distance of the CC of around 60 kpc from the center of the galaxy. The age of the CC is 4.5 Myr.

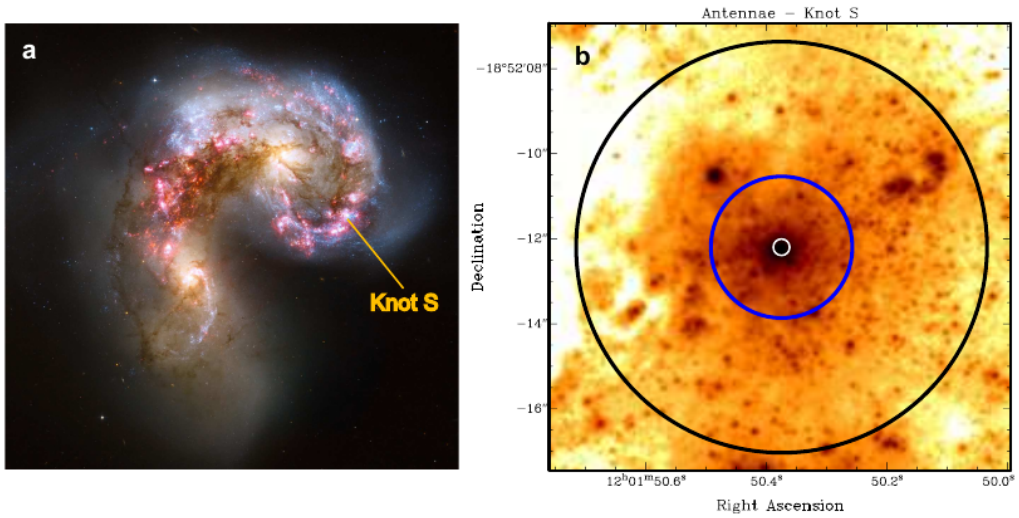

Figure 1.10: Antennae galaxies(NGC 4038 + NGC 4039), spiral galaxies interacting at a distance of 20 Mpc. (4.a) Shows the image of the central part of this system. The position of Knot S is labeled. (4.b) A HST ACS image in the F435W band of knot S. This is a CC, where it is possible to see an object already formed in the center. The circles in white (18 pc), blue(155 pc) and black(450 pc), denote the center object of the CC, the effective radius of the CC and the radius used to derive the Luminosity (by Whitmore et al (1999)), respectively. Image taken by Brüns 2013 PhD thesis, University of Bonn the data used in the plot was taken from the Hubble Legacy Archive.

1.5 Merging Star Cluster Scenario

Kroupa (1998) studied the dynamical evolution of CCs for the duration of 95 Myr and showed that in a CCs with a high density of star clusters the merger of this SCs is very possible. This merging process leads to a massive star cluster -the merger object- in the central part of a CC. This object can be interpreted as an early merger object. This scenario is called “merging star cluster scenario”. -the timescales and the effectiveness of this merger-process was studied in Fellhauer et al (2002) (CeMDA paper).
Fellhauer & Kroupa (2002a) (2002b) demonstrated that the merging star cluster scenario is able to produce merger objects with structural parameters similar to FFs and UCDs after a dynamical evolution of several Gigayears.

Brüns 2013 PhD thesis, University of Bonn did simulations for several Gigayears of a huge range of masses an sizes of CCs. The main parameters of her simulations, to investigate if the CCs are the progenitor of FFs and UCDs, are shown in the table 1.1. She varies different parameters and compares the results with the observations. She uses the values of M/L=2.3 for FF as no observational constrains on the M/L ratio of FF were available. This value was observed by Pryor & Meylan 1993 for 56 SC in the Milky Way.

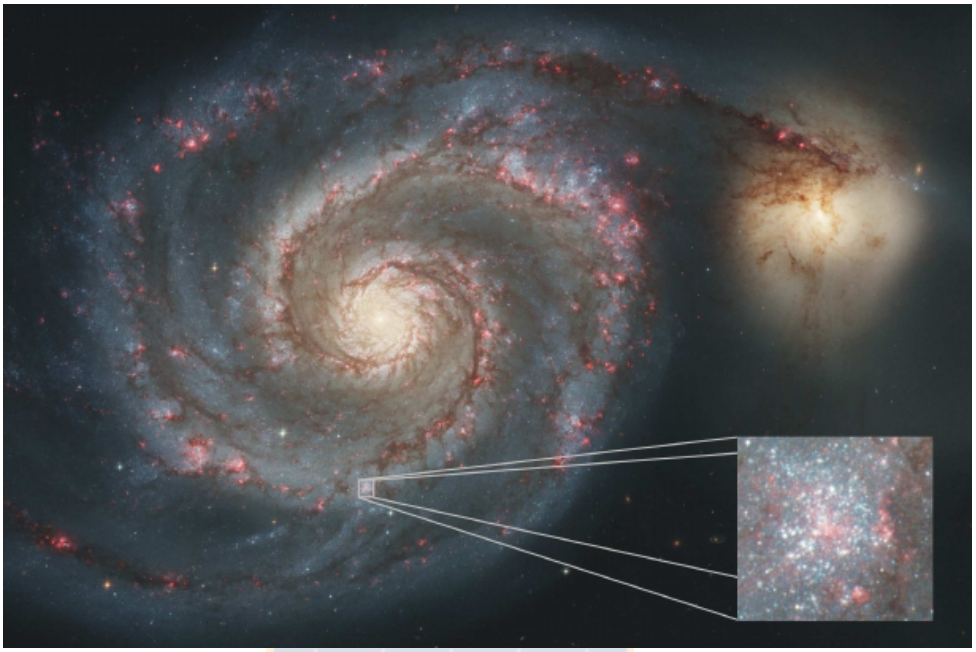

Figure 1.11: This figure is based on images taken from the HST public picture database. Formation of CC in a spiral galaxy forming during an interaction with a small companion galaxy (Like Whirlpool galaxy). There is an example of a CC in the zoom of one arm.

For UCD she uses the value M/L of 3 as an intermediate value between the typical mass to light ratios of about 2 and 4 of SCs and UCDs.
An important parameter in the studies of these systems is the Filling Factor parameter or α parameter which is defined as:

$$\alpha = \frac{R_{pl}^{SC}}{R_{pl}^{CC}} \tag{1.1}$$

Which is the ration between the Plummer radius of the SC and the Plummer radius of the cluster complex. So this parameter tells us how densely filled the system is.

Brüns 2013 PhD thesis, University of Bonn found that the type of the results depends mainly on the initial CC mass, the initial CC size and the external tidal field. Those 3 parameters are combined in the parameter β which is the ratio of the cut off radius (R_{cut}^{CC}) and the tidal radius of the CC (R_t^{CC}). The tidal radius depends on the CC mass and the strength of the tidal field:

$$\beta = \frac{R_{cut}^{CC}}{R_t^{CC}} \tag{1.2}$$

After comparing the results of the simulations with the observations, she found that the merging of stars clusters in CC is a possible formation scenario for FFs and UCDs, because the CC models evolve into stable objects having structural parameters comparable to those of the

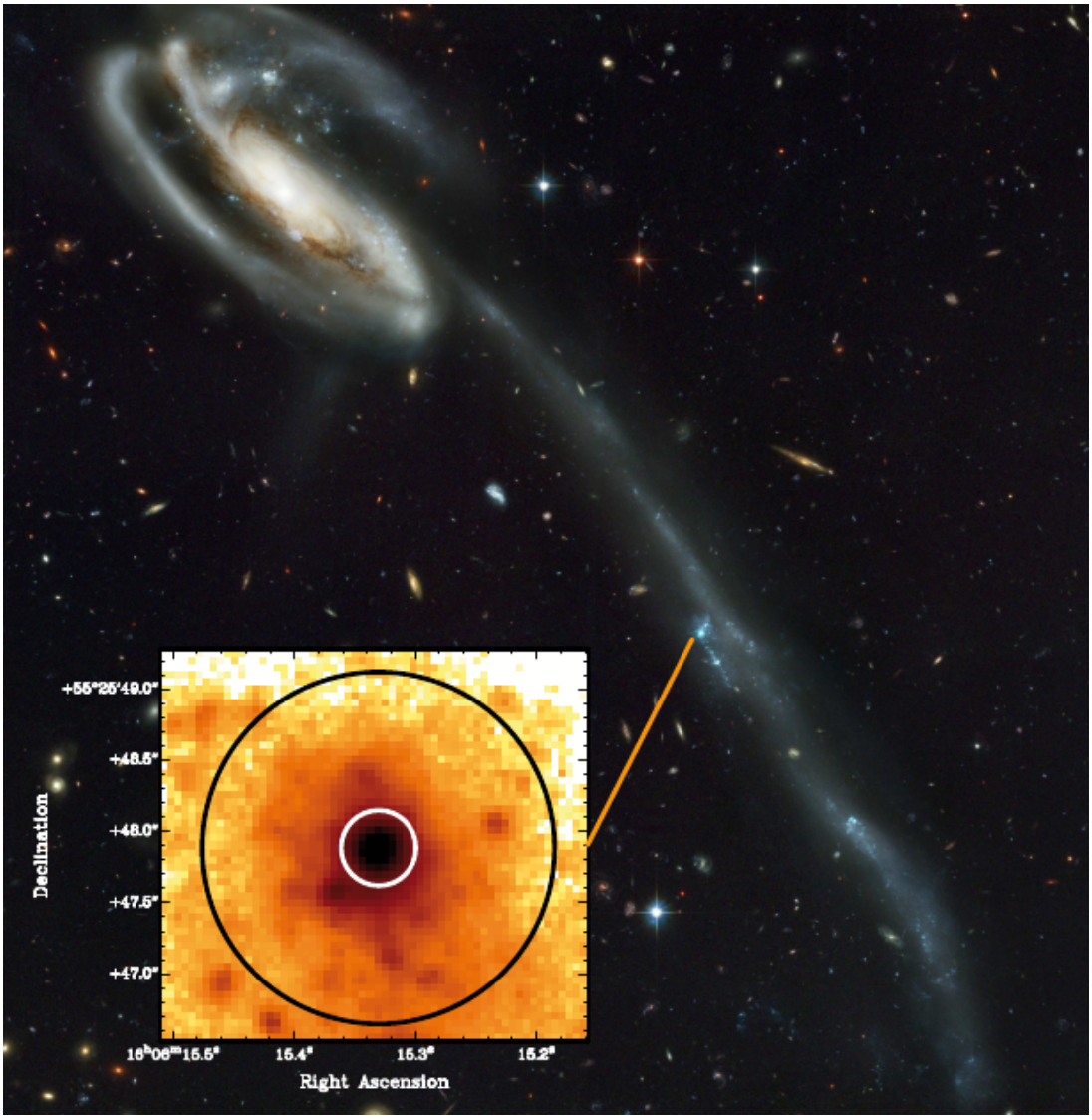

Figure 1.12: The main figure is taken from the HST public picture database and the enlargement is based on HST ACS data in the F435W band, taken from the Hubble Legacy Archive. This is the Tadpole Galaxy (USC10214). Here, it is possible to see an example of CC that forms within a tidal tail. In the blow-up, it is possible to see the most massive CC, which has a mass of the order 10^6 $M_{\odot}$, and an effective radius of 160 pc(white circle). This CC is located approximately 60 kpc from the center of the galaxy. The black circle (750 pc) covers the total extend of the CC. Image taken from Brüns 2013 PhD thesis, University of Bonn

observed objects.
"So, they are all part of the same formation process and they are, therefore united under the name Extended Stellar Dynamical Objects".

The resulting object is illustrated in Fig 1.13, which is a diagram of the destiny of compact or extended CC.

	FF	UCD
N_0^{sc}	100000	100000
N_0^{cc}	20	32
α	0.008	0.4,0.2,0.1,0.05,0.025
R_{cc}[pc]	85 - 240	10,20,40,80,160,240,360
Grids	64x64x64	128x128x128
$M_{cc}[M_\odot]$	$10^4 - 10^5$	$10^{5.5} - 10^8$
M/L	2.3 (Pryor & Meylan 1993)	3

Table 1.1: Main parameters of the simulations of Brüns 2013 PhD thesis, University of Bonn, to investigate if the CCs are the progenitor of FFs and UCDs. In the table N_0^{sc} is the number of particles that contains each SC, N_0^{cc} is the number of SCs in the simulation, α is the filling factor, R_{cc} is the size of the cluster complex, grids is the number of grids in the simulations, M_{cc} is the total mass in the simulation and M/L is the mass to light ratio. Source: From this work.

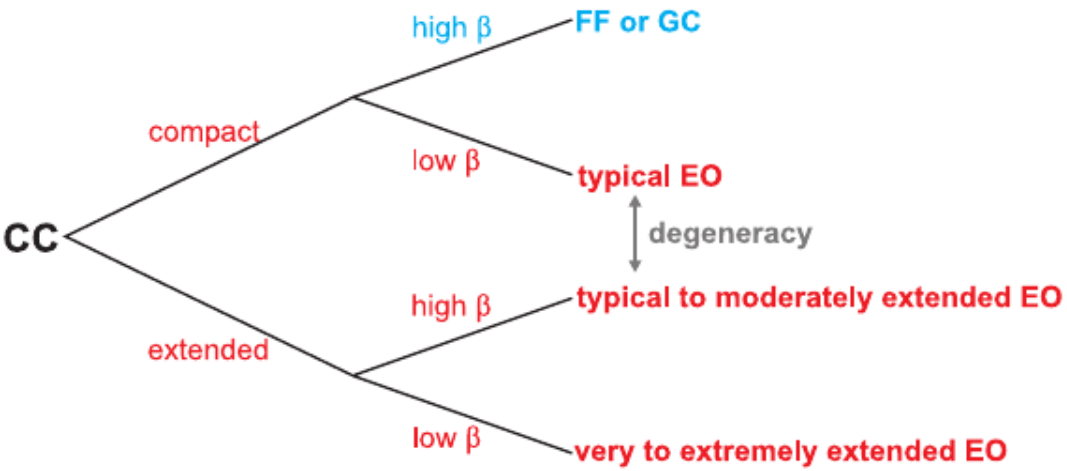

Figure 1.13: Diagram of the destiny of compact or extended CC. The colors represent the position in a galaxy where the simulations take place. Red represent simulations in the outer parts of the halo of the galaxies, and blue represents simulations in the disk and in the inner parts of the halo of the galaxies. Image taken from Brüns 2013 PhD thesis, University of Bonn.

Chapter 2

Superbox

SUPERBOX is a program making use of the particle-mesh technique with high resolution sub-grids and a nearest grid point (NGP) force-calculation scheme based on the second derivatives of the potential. SUPERBOX implements a fast low-storage Fast Fourier Transformation (FFT) algorithm, giving the possibility to work with millions of particles on desk-top computers. This code is efficient in various ways, for example:

- Avoids the limitation in spatial resolution encountered with standard particle mesh codes that employ only a single grid.
- The computational overhead is kept as slim as possible.
- The code is also memory efficient by using only one set of grids to treat galaxies in succession.

The basic idea behind SUPERBOX is to increase the resolution only at places where it is necessary, while simultaneously keeping the computational overhead as small as possible by using fixed nested grid-architecture, also the accuracy is improved by the use of nested high-resolution sub-grids and a linear force interpolation to the exact position of the particle inside a cell. SUPERBOX provides two higher-resolution levels of sub-grids, both grids stay focused on the galaxy. The medium-resolution grid contains an entire galaxy, and the high-resolution grid treats its core.
Another important feature of this code is the memory requirement of SUPERBOX scales both linearly with the particle number N_p, and with the number of grid-cells $N_{gc} = n^3$. In the particle-mesh technique the density of the particles is sampled on a grid covering the simulation area, and the Poisson's equation

$$\bigtriangledown^2 \Phi = 4\pi G\rho \tag{2.1}$$

in where Φ is the potential, G is the gravitational constant and ρ is the density, is solved on these

grid-based density to get the grid-based potential, Φ_{ijk}, using the FFT method and a suitable Green's function.

- Suitable Green's function: The usual geometry of the grid in a particle-mesh code is Cartesian and cubic. The standard Green's function, which describes the distances between cells,

$$H_{ijk} = \frac{1}{i^2 + j^2 + k^2} i, j, k = 0, ...n \tag{2.2}$$

  Where the grid-cell has unit length and n is the number of grid-cells per dimension and has to be a power of two.

- Deriving the density-grid: the first step is to locate the grid-point of each particle according to its position (x, y, z) and derive the density grid. To assign the mass of the particle to the density-grid covering the simulation are there are two possibilities:

  1. Nearest-grid-point scheme (NGP): assigns the whole mass of the particle to the grid-cell.
  2. Cloud-in-cell scheme (CIC): assigns a radius of half a cell length to each particle, and the mass of the particle is now distributed to the cell the particle is in and the surrounding cells according from the actual deviation of the particle position with respect to the center of the cell

  SUPERBOX still uses the NGP scheme, which results in a much faster assignment of the densities, Fig 2.1 show how this assignment looks like in two dimensions.

- The FFT - algorithm: gives the exact solution of the grid-based potential for a periodical system. For the exact solution of an isolated system, the size of the density-array has to be doubled $(2n)$, filling all inactive grid cells with zero density, and extending the Green's function in the empty regions, using:

$$\begin{aligned} H_{2n-i,j,k} &= H_{2n-i,2n-j,k} \\ &= H_{2n-i,j,2n-k} \\ &= H_{2n-i,2n-j,2n-k} \\ &= H_{i,2n-j,k} \\ &= H_{i,2n-j,2n-k} \\ &= H_{i,j,2n-k} \\ &= H_{i,j,k} \end{aligned}$$

  this provides the isolated solution of the potential in the simulated area between $i, j, k = 0$ and $n - 1$.

- Derivation of the forces: Once we have a grid-based potential of our simulation area, from this potential values the forces acting on each particle are derived via discrete numerical differentiation of the potential.

- Integrating the particles: the orbits of the particles are integrated forward in the time using the leap frog algorithm. SUPERBOX uses a fixed global time-step (the same time-step for all particles).

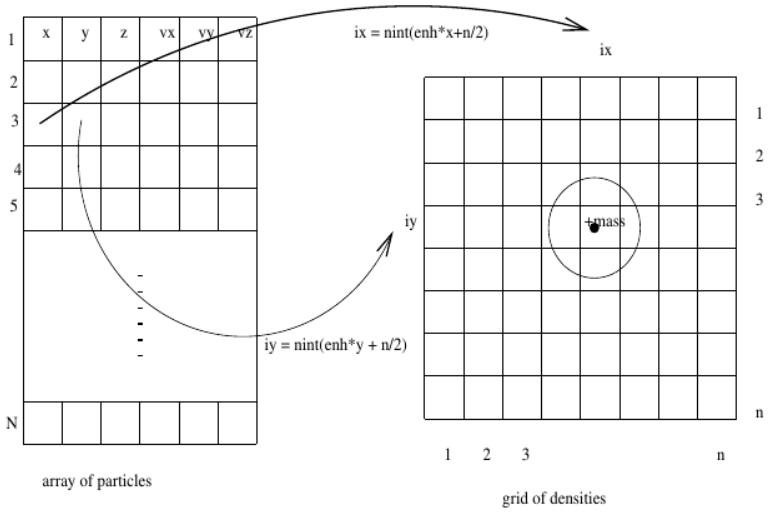

Figure 2.1: Two dimensional scheme that show the deriving density grid out of the particle positions. Image taken from Fellhauer et al 2000.

You can see how Superbox works in Fig 2.2a and Fig 2.2b. Fig 2.2a is a float chart of SUPERBOX taken by Fellhauer et al (2000). In this Fig you can see step by step how SUPERBOX works. Fig 2.2b is a Scheme of how SUPERBOX works taken from Brüns 2013 PhD thesis, University of Bonn, here you can see the three main blocks of how SUPERBOX works.

An important feature of SUPERBOX is the multi-grid structure. For each object, five grids with 3 different resolutions are used, this is possible by invoking the additivity of the potential Fig 2.3. The five grids are as follows:

- Grid 1: is the high-resolution grid which resolves the center of the galaxy. It has a length of $2 \times R_{\text{core}}$ in one dimension, with R_{core} the radius of high resolution grid centered in the object. In evaluating the densities, all particles of the galaxy within $r \leq R_{\text{core}}$ are stored in the grid.

- Grid 2: has an intermediate resolution to resolve the galaxy as a whole. The length is $2 \times R_{\text{core}}$, but only particles with $r \leq R_{\text{core}}$ are stored here, i.e. the same particles as are also stored in grid 1.

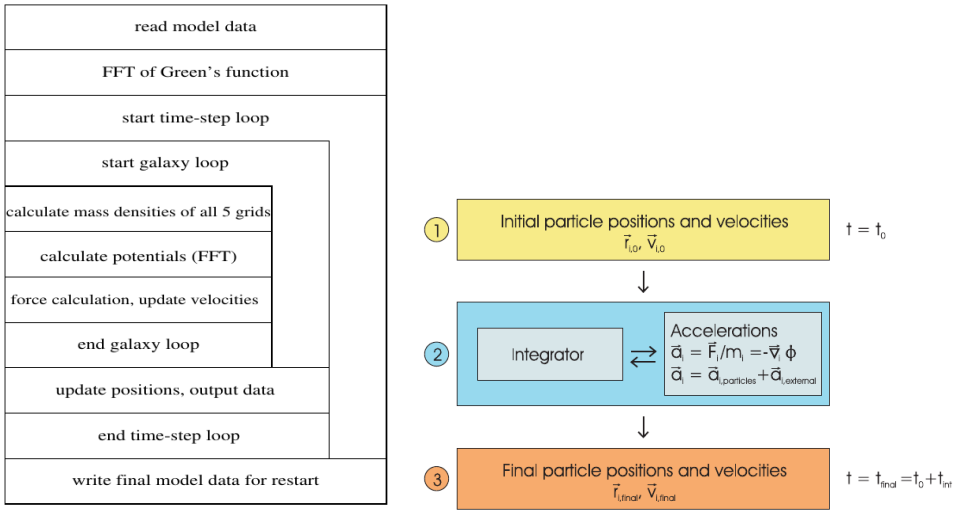

(a) Floart chart (b) Diagram of SUPERBOX

Figure 2.2: Float chart of SUPERBOX and diagram of the three main blocks of how SUPERBOX works. Image taken from Fellhauer et al 2000 and Brüns 2013 PhD thesis, University of Bonn, respectively.

- Grid 3: has the same size and resolution as a grid 2, but only contains particles with $R_{\rm core} < r \leq R_{\rm out}$.
- Grid 4: has the size of the whole simulation are, i.e. local universe with $2 \times R_{\rm system}$, and has the lowest resolution. It is fixed. Only particles of the galaxy with $r \leq R_{\rm out}$ are stored in grid 4.
- Grid 5: has the same size and resolution of grid 4. This grid treats the escaping particles of a galaxy, and contains all particles with $r > R_{\rm out}$.

Grids 1, 2 and 3 are focused on a common center of the galaxy and move with it though the local universe. All grids have the same number of cells per dimension, n, for all galaxies. Each of the grids has its associated potential Φ_i, with $i = 1, 2, ..., 5$ computed by the particle-mesh technique, and:

- For a particle in the range $r \leq R_{\rm core}$ the potentials of the grids 1,3 and 5 are used to calculate the acceleration.
- For a particle with $R_{\rm core} < r \leq R_{\rm out}$, the potentials of grids 2,3 and 5 are combined.
- If $r > R_{\rm out}$ then the acceleration is calculated from the potentials of grids 4 and 5.
- A particle with $r > R_{\rm system}$ is removed from the computation.

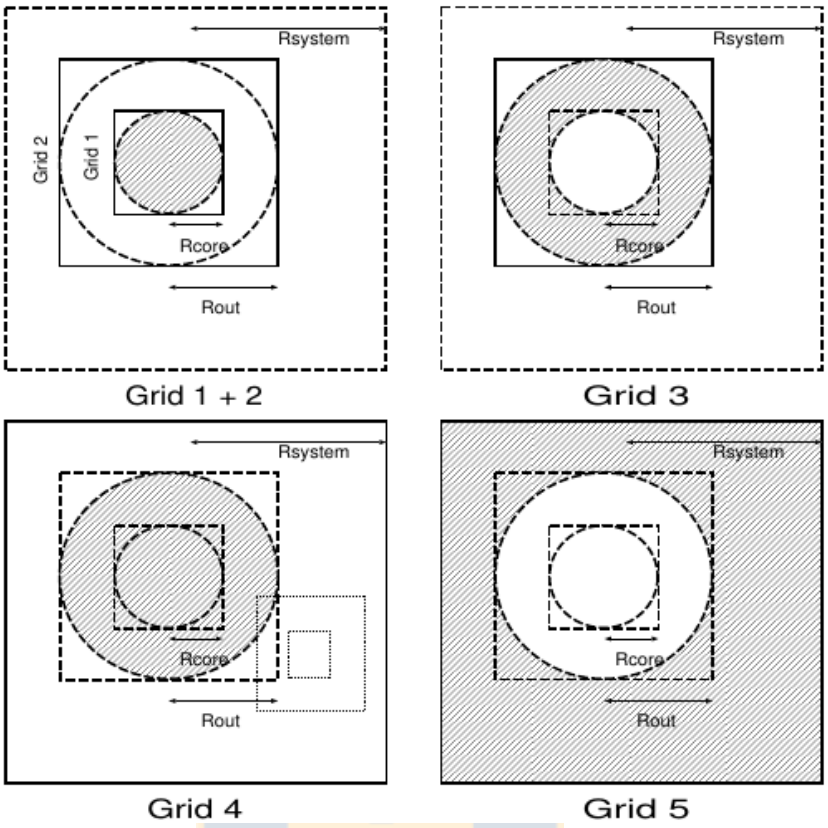

Figure 2.3: Multi-Grid structure of SUPERBOX. Image taken from Fellhauer et al. 2000.

Chapter 3

Method & Setup

We first repeat simulations similar to Brüns et al. (2011) to reach the regime of UCDs with masses similar to 10^6 or 10^7 M$\odot$ using the merging star cluster scenario (see figure 3.1). We divide this mass inside a cluster complex into 16 or 32 star clusters. We measure the parameters of the resulting UCDs and use them as input for our initial constituents to form a cE. For our cE models we divide the total mass of the cluster complex of 10^9 M$\odot$ into 64 UCDs. We perform models with and without tidal field (and different galactic distances). We will perform a large parameter study to see which initial conditions of cluster complexes will lead to final objects resembling cEs.

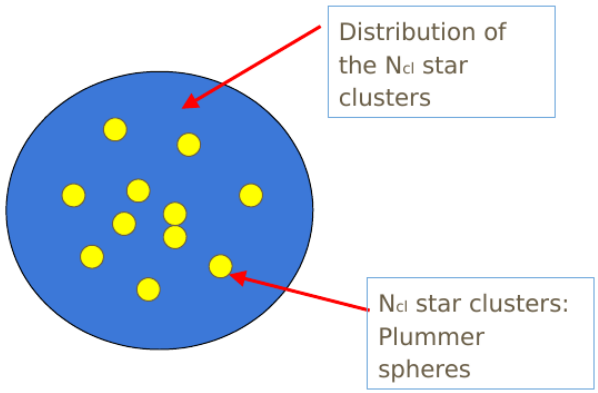

Figure 3.1: Initial conditions of the simulations. The Merging Star Cluster Scenario. Source: From this work.

3.1 Setup

In our simulation the stars clusters are modeled as Plummer spheres (Plummer 1911) with a Plummer radius given as R_{sc} and a cutoff radius of $R_{cut}^{sc} = 5R_{sc}$. The clusters themself inside the CC are distributed a in a Plummer distribution with a Plummer radius given as R_{cc} and $R_{cut}^{cc} = 5R_{cc}$.

To get a good resolution of the star clusters, the individual high resolution grids cover an entire star cluster, whereas the medium resolution grids of every star cluster embed the whole initial CC.

To have a circular orbit of the whole CC around the center of the galaxy, the velocities can be calculated knowing the equations (3.1) and (3.2) :

$$M = 4\pi \int_0^r \rho(r) r^2 dr \tag{3.1}$$

$$v^2 = \frac{GM(r)}{r} \tag{3.2}$$

This leads to different initial velocities at different distance to the galactic center (R_{gal}). In table 3.1 the initial velocity required for the cluster complex to obtain a circular orbit ($v_{circ.orbit}$) is displayed according to the distance to the center of the galaxy of the cluster complex (R_{gal} [kpc]).

R_{gal} [kpc]	$v_{circ.orbit}$
20	230
40	214
60	206.6
100	219.8
120	198

Table 3.1: Initial velocity required for the cluster complex to obtain a circular orbit ($v_{circ.orbit}$) according to each distance to the center of the galaxy of the cluster complex (R_{gal} [kpc]). Source: From this work.

3.2 Setup of the simulations with masses of 10^6 or 10^7 M⊙(EC, FFs and UCDs)

The first simulations we performed was with a mass of the system of 10^6 $M_\odot$, distributed into $N_0^{CC} = 16$ stars clusters, i.e each cluster has a mass of $M_{sc} = 62,500$ $M_\odot$ simulated by 100,000 particles. The stars clusters are modeled as Plummer spheres (Plummer 1911) with a Plummer radius of $R_{sc} = 4$pc and a cutoff radius of $R_{cut}^{sc} = 5R_{sc}$. The clusters inside the CC are distributed a in a Plummer distribution with R_{pl}^{cc}=50pc and $R_{cut}^{cc} = 5R_{cc}$.

We also did simulations for systems with the potential of the Milky Way, at different distances from the center, and with the same parameters explained before. These galactic radii are: 20 kpc, 40 kpc and 60 kpc.

Then we increased the number of clusters of the distribution at $N_0^{CC} = 32$, to explore the same scenarios explained before, but now with mass distributed in more constituent of the CC. So, now each star cluster has a mass of 31.250 Solar Masses.
After, we increase the total mass of the simulation from 10^6 M⊙ to 10^7 M⊙. All the parameters of each simulation are displays in the results section.

3.3 Setup of the simulations with masses of 10^9 M⊙(cEs)

For the simulations of cE we use a total CC mass of 10^9[$M_\odot$]. We distribute this mass into 64 UCDs, i.e. every UCD has with 15.625 × 10^6 $M_\odot$

$$M_{sc} = \frac{M_{cc}}{N_0} = \frac{10^9}{64}[M_\odot] = 15,625,000[M_\odot] \tag{3.3}$$

The simulations that we perform cover three different values for R_{gal}, R_{sc} and R_{cc}. In table 5.2 we show the values that we varied in the simulations.

R_{gal}[kpc]	20	60	100
R_{sc}[pc]	4	10	20
R_{cc}[pc]	50	100	200

Table 3.2: Parameters that we systematically vary in the simulations. The distance to the center of the galaxy of the CC (R_{gal}), the Plummer radius of the SCs (R_{sc}) and the Plummer radius of the cluster complex (R_{cc}). Source: From this work.

We perform simulations with all combinations, so we have 27 simulations.

To get a good resolution for the star clusters, the individual high resolution grids (R_{core}) cover an entire star cluster, whereas the medium resolution grids (R_{out}) of every star cluster embed the whole initial CC. In the table 3.3 is display the different grids that I use for different R_{sc}. The columns represent the Plummer radius of the SCs/UCDs, 0.01,0.004 and 0.02 kpc, respectively.

Grid	Size$_{R_{sc}=4pc}$	Size$_{R_{sc}=10pc}$	Size$_{R_{sc}=20pc}$
R_{core}[kpc]	0.08	0.2	0.4
R_{out}[kpc]	0.8	2	4
R_{system}[kpc]	160	160	170

Table 3.3: Values of the different grid in the simulations according to different initial Plummer radius of the SCs/UCDs. Individual high resolution grids (R_{core}), the medium resolution grids (R_{out}) and the grid that covers the whole simulation (R_{system}). Source: From this work.

Chapter 4

First simulations with masses of 10^6 or 10^7 M⊙(EC, FFs and UCDs)

In previous studies like Fellhauer (2002a,b), Fellhauer et al (2002)(CeMDA paper), Brüns et al (2009) and Brüns et al (2011), the merging star cluster scenario for masses up to 10^8 M⊙ has been studied. They find that the merging star cluster scenario is able to produce objects with properties of ECs, FFs and UCDs.
In this section I present similar simulations, to confirm that the merging star cluster scenario is able to produce extended objects.

The simulations performed had a system mass of 10^6 $M_\odot$, distributed into $N_0^{CC} = 16$ stars clusters, where each one contains 100.000 particles. Then we increase the N_0^{CC} from 16 to 32. And the last one has a initial mass of the distribution of 10^7 $M_\odot$. (see section 3.2)

The results of the simulations show similar objects to the previous ones found by studies in this topic (for example Brüns & Kroupa 2012), regarding to final parameters like, effective radius ($R_{\rm eff}$), mass, central surface brightness (Σ_0), shape and central velocity dispersion (σ_0).

The data points for $R_{\rm eff}$, Σ_0 and σ_0 were obtained with an IDL script. We give to the script in IDL the position and velocities of every particles in the final object. IDL take the position of all particles in the final object and make a position map counting the number of particles inside each pixel, which gives us the mass/arcsec^2. With the M/L that we choose in the script (in this case 1), we transform these values to luminosities and magnitudes. In this way IDL is able to make diagrams of surface brightness with color bars.
IDL also produces radial profiles of surface brightness and line of sight velocity dispersion, taking the medium value inside concentric circles that begins in the center of the object (0 pc) and increase its radius, until a chosen value in the script (in this case 1.5 kpc).

To fit our data-points, we use a Sersic profile:

$$I(R) = I_e exp\left\{-b_n\left[\left(\frac{R}{R_e}\right)^{1/n} - 1\right]\right\} \tag{4.1}$$

Here I_e is the intensity at the effective radius R_e that encloses half of the total light from the model. The constant b_n is defined in terms of the third and final parameter n which describes the 'shape' of the light-profile. b_n satisfy the next equation which relate the incomplete Gamma function (γ) and the Gamma function (Γ)

$$\gamma(2n; b_n) = \frac{1}{2}\Gamma(2n) \tag{4.2}$$

The ellipticity is obtained from IRAF. In IRAF we use the ELLIPSE routine, from where we can obtain the ellipticity value at different radii for each isophote, The chosen value for the radius of the isophote, for the analysis the ellipticity is approximately 100 pc. In all simulations, the merging process leads to a stable object.

In Fig 4.1 we show the characteristics of the final objects until a radius of 1.5 kpc, of 5 different simulations. The left panel is the shape of the final object with a color bar for the magnitude of the surface brightness, the center panel is the plot of the surface brightness profile and the right panel is the velocity dispersion, under each set of images the initial conditions of the simulation is described. The size of the SC is R_{sc}=4 pc, and of the CC is R_{cc}=50 pc in all simulations.

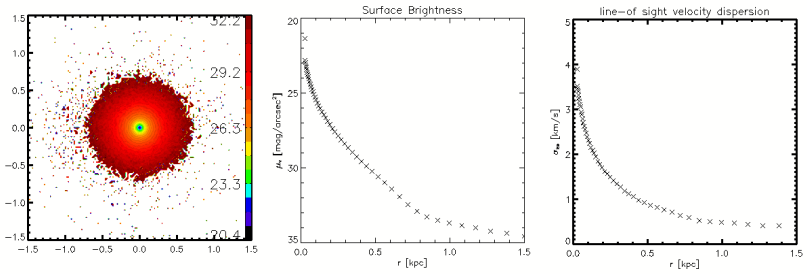

(a) Sim4:$1 \times 10^6 M_\odot$,N^0=16

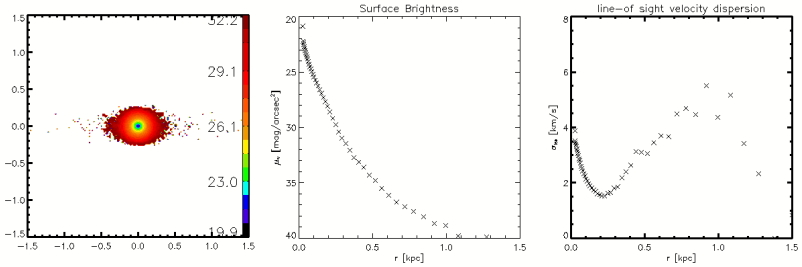

(b) Sim12:$1 \times 10^6 M_\odot$,N^0=16,R_{gal}=40(kpc),v_0=218(km/s)

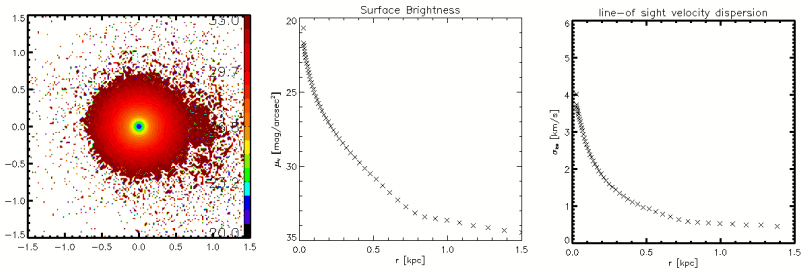

(c) Sim13:$1 \times 10^6 M_\odot$,N^0=32

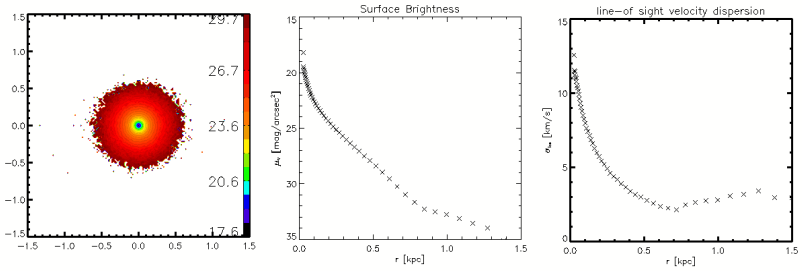

(d) Sim14:$1 \times 10^7 M_\odot$,N^0=16

Figure 4.1: Characteristics of the final object until a radius of 1.5 kpc, the left panel is the shape of the final object with a color bar for the magnitude of the surface Brightness, the center panel is the plot of the surface brightness and the right panel is the velocity dispersion, under each set of images is the initial conditions of the simulation. The size of the SC is R_{sc}=4[pc], and of the CC is R_{cc}=50[pc] in all simulations. Source: From this work.

Almost all simulations are in good agreement with the results obtained by the previous works (for example Brüns 2013 PhD thesis, University of Bonn).
The parameters the simulations and results are displayed in Table 4.1. The left side of the table 4.1 show the initial parameters of the simulation and separated by a double line the characteristic of the resulting object.
In the left side we can see the total mass ($M_\odot$), the number of SCs(N^0), the Plummer radius of each SC (R_{sc}), the plummer radius of the distribution or CC(R_{cc}) and the distance to the center of the galaxy of the distribution (R_{gal}) in the simulation.
In the right side we see the number of SCs in the merger object ($N_{0,merger}$), the number of particles, the final effective radius ($R_{\rm eff}$), the ellipticity, the central velocity dispersion(σ_0) and the central surface brightness(Σ_0) of the merger object

The result of the Simulation4, 12 and 13, are consistent with an Extended Objects (EC), according to their mass, size, ellipticity, σ_0 and Σ_0. (see Table C.2 and C.6 in Brüns 2013 PhD thesis, University of Bonn)

The results of Simulation14 are in good agreement with an UCD, the mass of UCDs is approximately 10^7 and the sizes between 10 and 100 pc. σ_0 in the simulations of Brüns 2013 PhD thesis, University of Bonn range between 8 to 18 [km/s] (see Table C.4 in Brüns 2013 PhD thesis, University of Bonn).

Name	Mass[$M_\odot$]	N^0	R_{sc}[pc]	R_{cc}[pc]	R_{gal}[kpc]	$N_{0,merger}$	Particles	M_{merger}[$M_\odot$]	$R_{\rm eff}$[pc]	Ellipticity	σ_0[km/s]	Σ_0[mag/arcsec^2]
Sim4	1×10^6	16	4	50	-	14	999687	6.2×10^5	67.7 ± 0.3	0.019	3.9087	20.3507
Sim12	1×10^6	16	4	50	40(v_0=218[km/s])	13	1300000	8.1×10^5	30.5±0.2	0.082	3.897	19.9233
Sim13	1×10^6	32	4	50	-	32	3199720	9.9×10^5	20.7±0.6	0.041	4.0411	20.0054
Sim14	1×10^7	16	4	50	50(v_0=219.3[km/s])	16	1599976	9.9×10^6	8.4±0.7	0.046	12.6734	17.5842

Table 4.1: Table first results. In the left side of the table the initial parameters of the simulation are shown and separated by a double line the characteristics of the result object.
In the left side we can see the total mass ($M_\odot$), the number of SCs(N^0), the Plummer radius of each SC (R_{sc}), the Plummer radius of the distribution or CC(R_{cc}) and the distance to the center of the galaxy of the distribution (R_{gal}) in the simulation.
In the right side we see the number of SCs in the merger object ($N_{0,merger}$), the number of particles, the final effective radius ($R_{\rm eff}$), the ellipticity, the central velocity dispersion(σ_0)-which is the dispersion of velocities about the mean velocity of the stars in the final object- and the central surface brightness(Σ_0) of the merger object. Source: From this work.

Chapter 5

Simulations of cE

We perform in total 81 simulations, where we varied R_{sc}, R_{cc} and R_{gal} (this gives us 27 simulations, which we perform 3 times with different random numbers, resulting in 3 sets of initial positions and velocities for the SCs/UCDs, for statistics).
We show in Table 5.1 the orbital parameters for the different distances of the distribution to the center of the galaxy. Here ,R_{gal} is the distance to the center of the galaxy of the distribution of SCs/UCDs, $v_{\rm circ.orbit}$ is the initial velocity of the distribution to have a circular orbit, $t_{\rm int}$ is the integration time, $T_{\rm orb}$ is the orbital period and it is the time that take the distribution in complete one period around the center of the galaxy and is given by $2\,\pi\frac{R_{\rm gal}}{v_{\rm circ.orbit}}$ and $N^0_{\rm revolutions}$ is the number of revolutions and it's given by $\frac{t_{\rm int}}{T_{\rm orb}}$.

R_{gal}[kpc]	$v_{\rm circ.orbit}$	$t_{\rm int}$[Gyr]	$T_{\rm orb}$[Gyr]	$N^0_{\rm revolutions}$
20	230	10	0.534	18.726
60	206.6	10	1.778	5.624
100	219.8	10	2.795	3.577

Table 5.1: Orbital parameters of a circular orbit for a logarithmic potential. R_{gal} is the distance to the center of the galaxy of the distribution of SCs/UCDs. $v_{\rm circ.orbit}$ is the initial velocity of the distribution to have a circular orbit. $t_{\rm int}$ is the integration time and show the total time simulated. $T_{\rm orb}$ is the orbital period and it is the time that take the distribution in complete one period around the center of the galaxy $N^0_{\rm revolutions}$ is the number of revolutions and it's given by the ratio between t_{int} and T_{orb}. Source: From this work.

The data points for $R_{\rm eff}$, Σ_0 and σ_0 were obtained with an IDL script as we explained in Chapter 4. The ellipticity is obtained from IRAF. In IRAF we use the ELLIPSE routine, from where we can obtain the ellipticity value at different radii for each isophote, The chosen value for the radius of the isophote, for the analysis of the ellipticity is approximately 100 pc.

The setup and results are displayed in Table 5.2. The name of the simulations is according to the size of a single SC/UCD(4-A, 10-B and 20-C [pc]), the size of the distribution (CC)(50-a, 100-b and 200-c [pc]) and the distance to the center of the galaxy of the distribution(20-1,60-2 and 100-3 [kpc]). For example SimAa1 means that the SC in the simulation has a Plummer radius of 4 pc, the Plummer radius of the CC is 50 pc and the distance to the center of the galaxy is 20 kpc.

In Table 5.2 you can see the setup of the simulations, the size of a single SC/UCD(R_{sc}), the size of the distribution or CC (R_{cc}) and the distance to the center of the galaxy of the distribution(R_{gal}) and separated with a double line are the characteristic of the final object, the number of the SCs in the merger object(N_{merger}), the total mass in the final object (M_{merger}), the final effective radius(R_{eff}), the ellipticity of the final object, the velocity dispersion (σ_0) and the central surface brightness of the final object(Σ_0). The mean value for one quantity of the final objects was obtained with the results of the average of three different initial distributions of the GC in the CC. And the error was obtained with the standard deviation of these three values.

In the table 5.2 we could see that almost all parameters of the final object are similar to the parameters of cEs. This will be discussed in detail in sections 5.1, 5.2, 5.3, 5.4 and 5.5 .

Name	R_{sc}[pc]	R_{cc}[pc]	R_{gal}[kpc]	N_{merger}	$M_{merger}[M_\odot]$	$R_{\rm eff}$[pc]	Ellipticity	σ_0[km/s]	Σ_0[mag/arcsec^2]
SimAa1	4	50	20	61.6±0.5	960170364.5±13237238.2	131.4±13.4	0.1±0.09	56.6±0.8	15.6±0.1
SimAa2	4	50	60	62.3±1.5	951079739.5±38641360.9	140±10	0.05±0.04	56.2±0.8	15.8±0.2
SimAa3	4	50	100	62.6± 1.5	915743229.1±15037357.1	138.7±10.3	0.08±0.07	55.5±0.4	15.8±0.2
SimBa1	10	50	20	63.6±0.5	994780000±9027775.9	98.7±11.3	0.1±0.03	72±4.3	14.9± 0.2
SimBa2	10	50	60	63.6±0.5	991880312.5±11140963.3	100.2±11.3	0.09±0.02	71.4±3.3	14.9±0.2
SimBa3	10	50	100	63.6±0.5	969046927±19194386.7	100.8±11.2	0.09±0.02	71.2±3.6	14.9±0.2
SimCa1	20	50	20	64	999704166.6±507393	89.9±4.4	0.09±0.07	82.3±4.1	14.9
SimCa2	20	50	60	64	995881093.7±5242532.5	89.8±4.4	0.14±0.01	82.6±4.1	14.9± 0.13
SimCa3	20	50	100	64	990504270.8±5847477.5	89.9±4.5	0.17±0.08	81.6±2.1	14.9±0.07
SimAb1	4	100	20	50.3±11.5	785328489.5±178751267.8	172.7±30.2	0.18±0.02	50.2±8.5	16.1±0.4
SimAb2	4	100	60	47.3±14.5	720880208.3±207221923.6	174.7±36	0.18±0.04	49.6±9.1	16.1±0.4
SimAb3	4	100	100	50±12	716185677±147547649.7	178.7±35.4	0.21±0.16	49.2±9.3	16.1±0.4
SimBb1	10	100	20	64	1000000000	119.5±26.8	0.16±0.08	68.1±5.4	15 ±0.2
SimBb2	10	100	60	64	999591354.1±393294.5	118.3±25.3	0.17±0.12	67.5±4.4	15.1±0.2
SimBb3	10	100	100	64	993577447.9±5525130.9	118.6±25.4	0.1±0.05	66.1±6.2	15.1±0.2
SimCb1	20	100	20	64	999997500±4330.1	115.3±8.3	0.19±0.18	71.7±5.4	15.2±0.1
SimCb2	20	100	60	64	999439166.6±951516.4	115.2±8.2	0.19±0.13	71 ±4.6	15.2±0.2
SimCb3	20	100	100	64	997910312.5±619138.5	115.2±8.3	0.09±0.09	71.1±4.8	15.2±0.2
SimAc1	4	200	20	26±13	405705364.5±202628674.5	242.4±30.4	0.2±0.09	27.1±8.6	17.3±0.2
SimAc2	4	200	60	26±13	388928281.2±189490314.7	251.1±43.2	0.18±0.08	26.5±7.3	17.2±0.2
SimAc3	4	200	100	25±12.1	348225000±163560704.4	257.4±23.9	0.18±0.03	26.2± 7.2	17.2±0.2
SimBc1	10	200	20	64	1000000000	197.2±62.6	0.13±0.03	52.9±4.5	15.5±0.2
SimBc2	10	200	60	64	999707916.6±502928.6	199±67.8	0.14±0.03	51.9±5.9	15.5±0.1
SimBc3	10	200	100	64	995186770.8±1328617.7	201.5±65.5	0.14±0.02	51.4±4.6	15.4±0.1
SimCc1	20	200	20	64	1000000000	192.7±49.3	0.32±0.11	55.1±6	15.9±0.3
SimCc2	20	200	60	64	999921875±135316.4	190.8±44.9	0.24±0.13	54.4±5.7	15.9±0.2
SimCc3	20	200	100	64	998321666.6±1226579	190.5 ±42.4	0.21±0.14	53.9±5.5	15.9±0.3

Table 5.2: Table results of simulations of cE. The name of the simulations is according to the size of a single SC/UCD(R_{sc}), the size of the distribution or CC (R_{cc}) and the distance to the center of the galaxy of the distribution(R_{gal}). In the table you can see the number of the SCs in the merger object(N_{merger}), the total mass in the final object (M_{merger}), the final effective radius($R_{\rm eff}$), the ellipticity, the velocity dispersion (σ_0) and the central surface brightness of the final object(Σ_0). Source: From this work.

In Fig 5.1, 5.2 and 5.3 we show characteristics of final objects until a radius of 1.5 kpc, of 9 differents simulations. The left panel is the shape of the final object with a color bar for the magnitude of the surface brightness, the center panel is a plot of the radial profile of surface brightness and the right panel is the radial profile of the line-of-sight velocity dispersion, under each set of images the initial conditions of the simulation are given. This simulations are taken as example from the 3 simulations where the only difference is the initial placement of the SCs/UCDs. Under each set of the 3 figures you can see the name of the simulation and the initial parameters of it.

In 5.1, 5.2 and 5.3 the $R_{\rm eff}$ of the final object should decrease while we increase the initial size of the SCs/UCDs (R_{sc}) (as we will explain in detail in section 5.2) but in Figure 5.2a and 5.3a it is clear that the first simulation (Sim91) and (Sim100) are smaller than the two below

them. This behavior will be explaind in the follows section 5.1 and 5.2.
Also the only difference between Fig 5.1, 5.2 and 5.3 is the initial size of the distribution R_{cc}=50 pc, R_{cc}=100 pc and R_{cc}=200 pc, respectively, so each set of objects in the figs should be bigger than the previous one, because the R_{eff} of the object and the initial size of the distribution R_{cc} are proportional which will be explained in section 5.2.

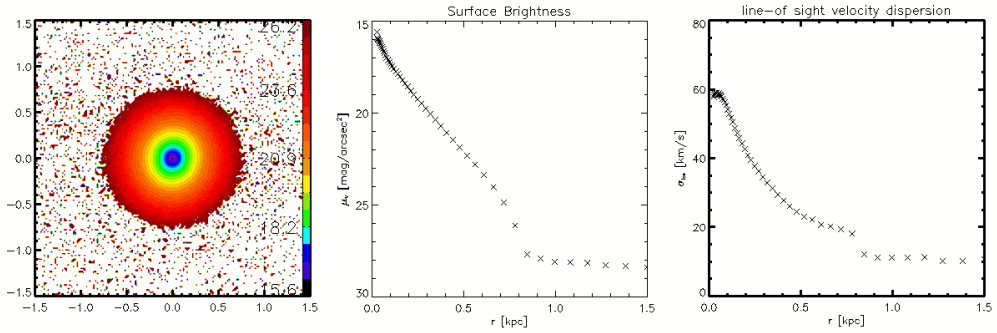

(a) Sim82: R_{sc}=4 pc, R_{cc}=50 pc

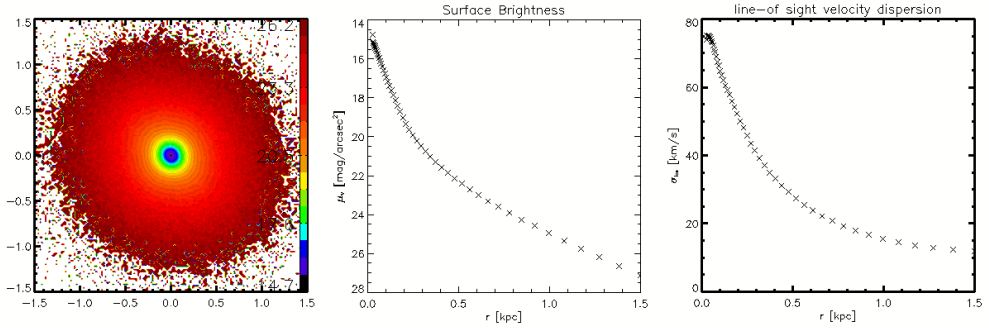

(b) Sim85: R_{sc}=10 pc, R_{cc}=50 pc

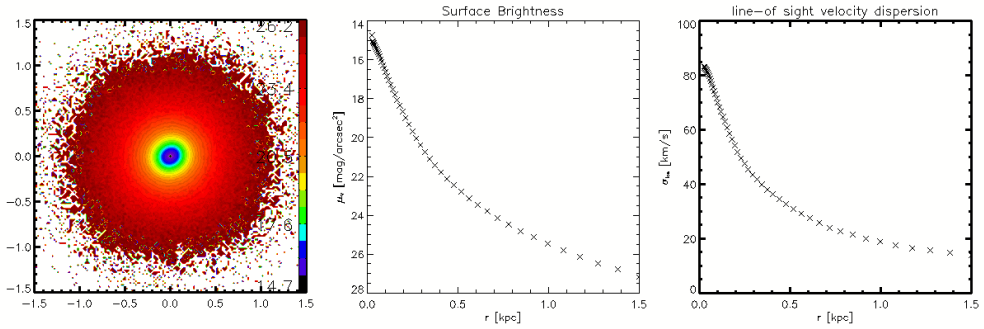

(c) Sim88: R_{sc}=20 pc, R_{cc}=50 pc

Figure 5.1: Characteristics of the final object until a radius of 1.5 kpc, the left panel is the shape of the final object with a color bar for the magnitude of the surface brightness, the center panel is the plot of the radial profile of the surface brightness and the right panel is the radial profile of the velocity dispersion, under each set of images is the initial conditions of the simulation. The simulations showed are the Sim82 with characteristic in Table 5.2 of SimAa2, Sim85 with characteristic of SimBa2, and Sim88 with characteristic of SimCa2. The R_{eff} of the final object decrease while we increase the initial size of the SCs/UCDs (R_{sc}) (as we will explain in detail in section 5.2). Source: From this work.

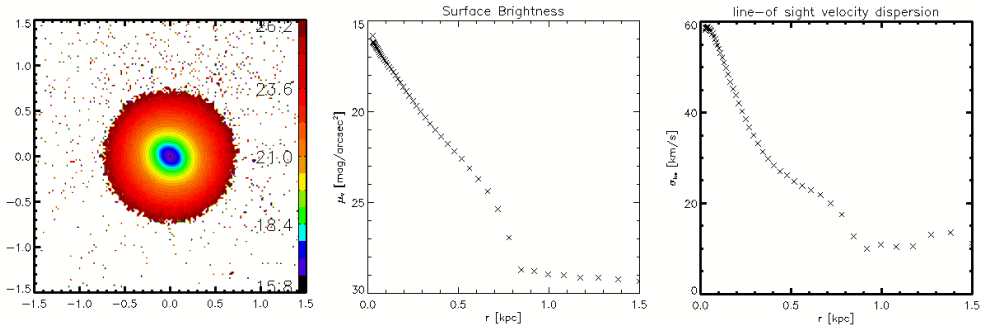

(a) Sim91: R_{sc}=4 pc, R_{cc}=100 pc

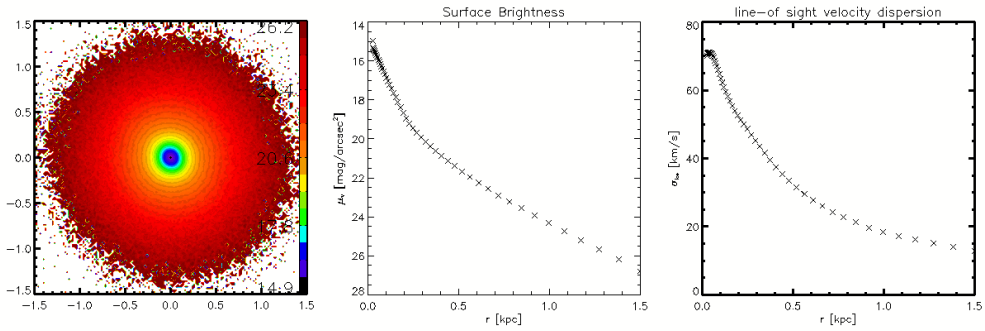

(b) Sim94: R_{sc}=10 pc, R_{cc}=100 pc

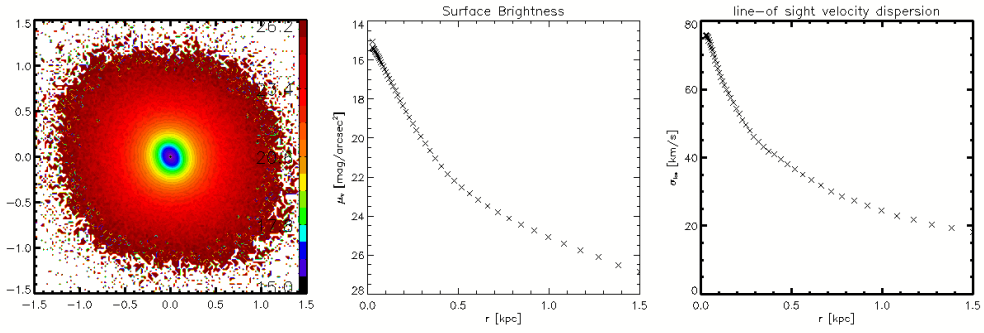

(c) Sim97: R_{sc}=20 pc, R_{cc}=100 pc

Figure 5.2: Same as Fig 5.1 but here the simulations shown are the Sim91 with characteristic in Table 5.2 of SimAb2, Sim94 with characteristic of SimBb2, and Sim97 with characteristic of SimCb2. The only difference is the size of the distribution (R_{cc}=100(pc)). So these objects are bigger than the analogous objects from Fig 5.1 this will be explained in section 5.2. Source: From this work.

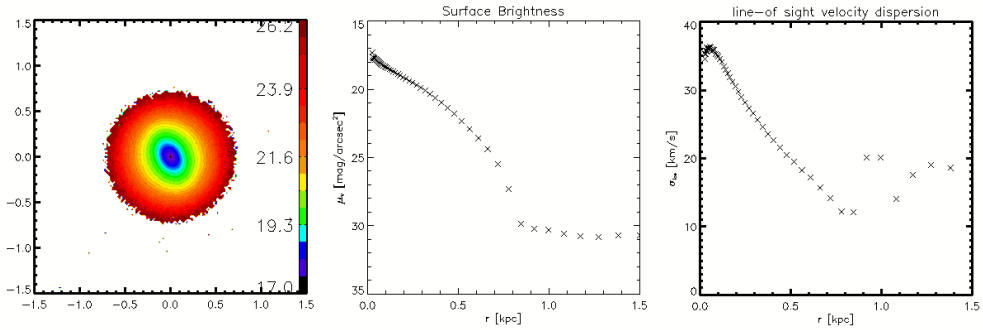

(a) Sim100: R_{sc}=4 pc, R_{cc}=200 pc

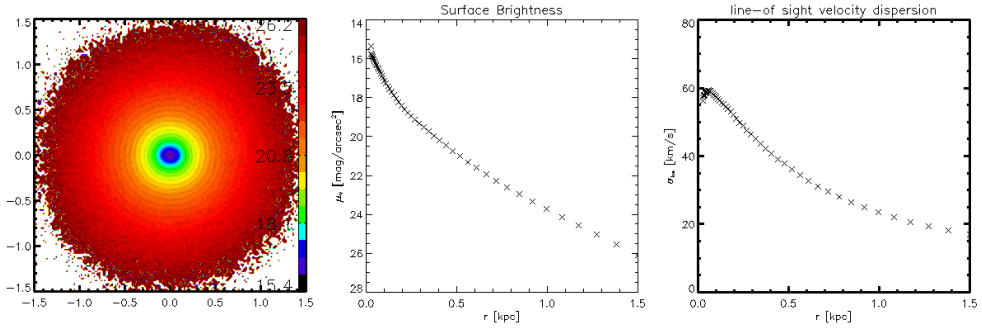

(b) Sim103: R_{sc}=10 pc, R_{cc}=200 pc

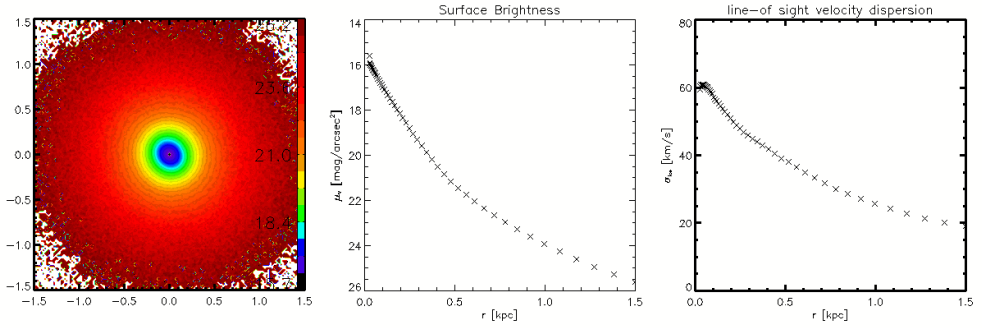

(c) Sim106: R_{sc}=20 pc, R_{cc}=200 pc

Figure 5.3: Same as Fig 5.1 but here the simulations shown are the Sim100 with characteristic in Table 5.2 of SimAc2, Sim103 with characteristic of SimBc2, and Sim106 with characteristic of SimCc2. The only difference is the size of the distribution (R_{cc}=200(pc)). So these objects are bigger than the analogous objects from Fig 5.1 and Fig 5.2 this will be explained in section 5.2. The $R_{\rm eff}$of the final object should decrease while we increase the initial size of the SCs/UCDs (R_{sc}) (as we will explain in detail in section 5.2), but here it is clear than the first simulation (Sim100) just like 5.2a are smaller than the two below them. This behavior will be explained in section 5.1 and 5.2. Source: From this work.

5.1 SCs/UCDs in the merger object

In Fig 5.4 we show the number of star clusters/UCDs which take part in the merging process and end up in the final object as a histogram (the total number of simulations is 81).

The result show a low merger rate when α is low or when β is high: The ratio of SCs/UCDs that merge, depends strongly in the α parameter. With high values of α the SCs/UCDs overlap right from the beginning, in the other hand with low values of α we start with a distribution of SCs/UCDs in where the merger of these SCs/UCDs stars to hapend in different parts of the CC, this second process do not guaranty the merger of each small-merger object with the biggest one, and these small-merger objects and the isolated end up "surviving" in the simulation.
Also it possible that some SC are located outside or are on an orbit which has an apo-center outside the tidal radius of the CC distribution and are stripped by the tidal forces of the galaxy.

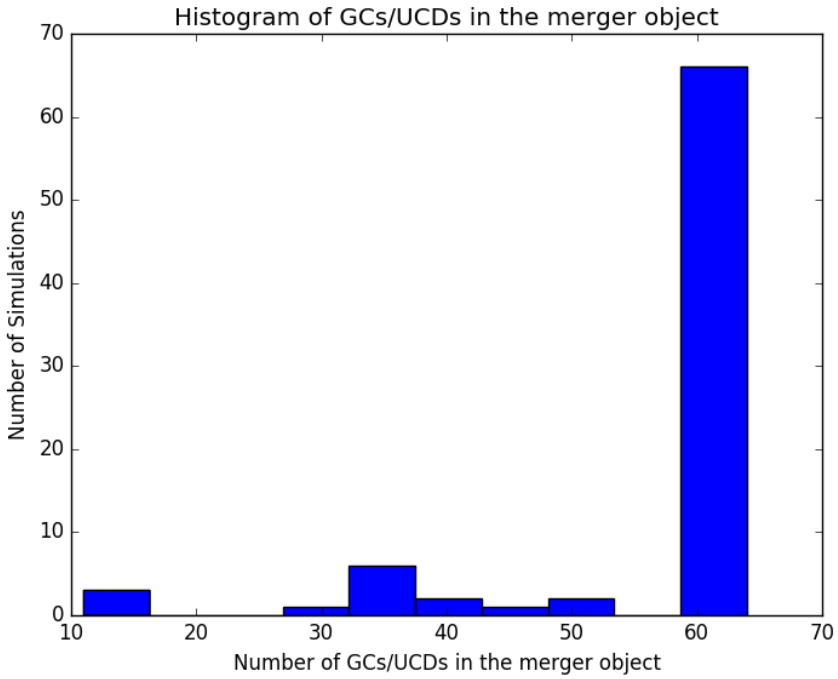

Figure 5.4: Histogram of numbers of SCs/UCDs in the merger object. The total number of simulations is 81. Simulations in where the merger object contain less than 50 SCs/UCDs are simulations with initial conditions of, $R_{sc} = 4$ pc, $R_{cc} = 200$ pc or $R_{sc} = 4$ pc, $R_{cc} = 100$ pc. Source: From this work.

This fraction of SCs/UCDs that not merge is bigger and significant only in the cases where the initial size of the SCs/UCDs is 4 pc and the initial size of the CC is 100 pc and 200 pc (Fig 5.4). This small number of SCs/UCDs in the final object is due the huge difference of sizes between SCs/UCDs and the CC. In both cases, approximately 50% of the initial SCs/UCDs merge, the rest that are still isolated follow their own orbit. An example of this is shown in Fig 5.5. Which is the orbits of some GCs/UCDs in Simulation99 which parameters correspond

to SimAc1, in where it is possible to see the SCs/UCDs orbiting, but not interacting with the merging object or the others SCs/UCDs.

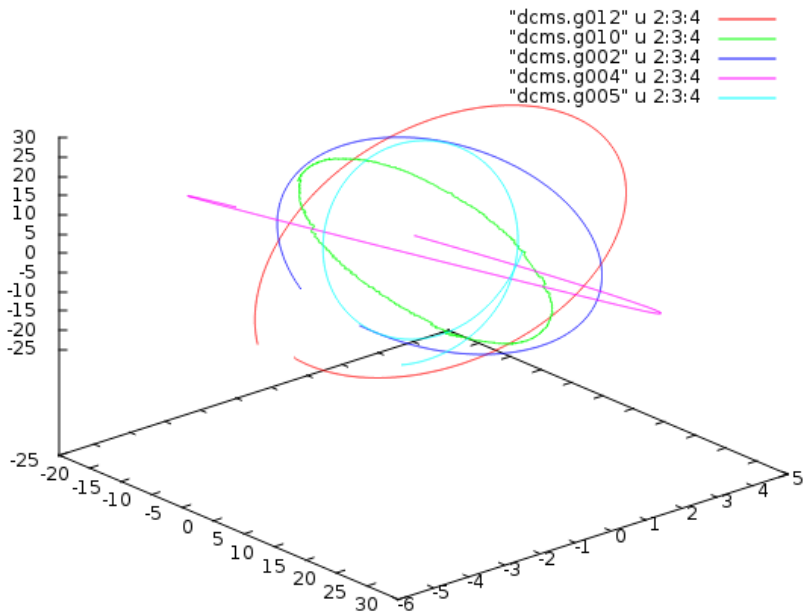

Figure 5.5: Simulation99, here it is possibly to see the SCs/UCDs orbiting, but not interacting with the merging object or the others SCs/UCDs. The initial parameters of this simulations are R_{sc}=4 pc, R_{cc}=200 pc, R_{gal}=20 kpc. Source: From this work.

In Fig 5.6 an example of a system in interaction is showed. Here it is possible to see the UCDs orbiting and interacting with the merger object and ending up in only one object after a dynamical evolution.

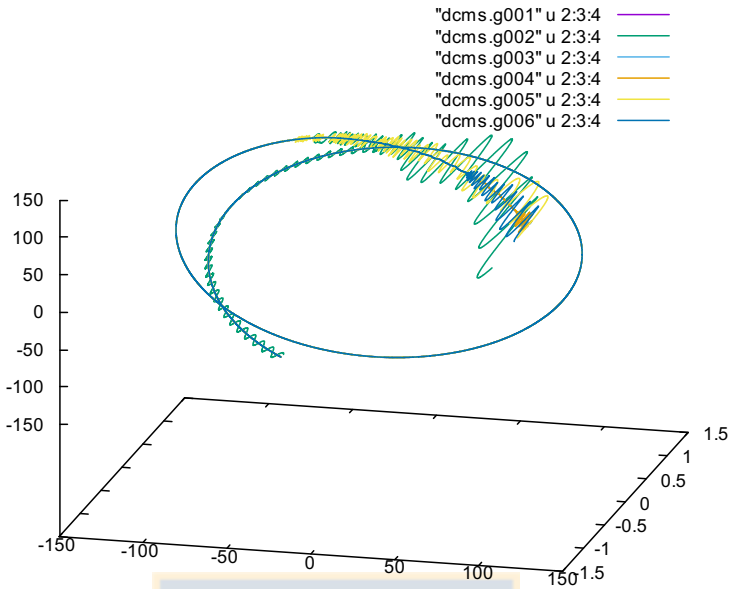

Figure 5.6: Simulation104, here it is possibly to see the SCs/UCDs interacting with the merging object. The initial parameters of this simulations are R_{sc}=10 pc, R_{cc}=200 pc, R_{gal}=100 kpc. Source: From this work.

In the cases when the ratio of merger in the simulation is too small we could rule out this final object of being cE, only because of the mass criteria. In this cases the mass is only half of what need to have to be a cE.

5.2 Effective radius of the final object(R_{eff})

To obtain R_{eff} we fit the data points of the radial surface brightness with a Sersic function. In this section we present the effective radii of the results of all 81 simulations.

In 5.7 we show the resulting effective radii as function of the galactic distance. The 3 panels show from left to right the results for SC/UCD with R_{sc}=4, 10 and 20 pc, respectively. In each panel the solid line is associated with CC radii of R_{cc} = 50 pc, the dotted line represents R_{cc} = 100 pc and the dashed line R_{cc} = 200 pc. The data point are mean values calculated from 3 realizations of these parameters with the associated 1 σ deviation as error-bars.
As a result we see almost horizontal lines, i.e. the final effective radius does not depend on the distance of the CC to the galactic center. Furthermore, we see almost no difference between the 3 panels, which points towards an independence of the final R_{eff} from the chosen size of the SCs/UCDs. Only in the case of small SCs (R_{eff}=4 pc) we obtain same slightly higher effective radii.
What we do see is an obvious dependence on the chosen scale-length of the CC distribution, i.e. the larger the Plummer radius of the CC, the larger the effective radius of the final cE.

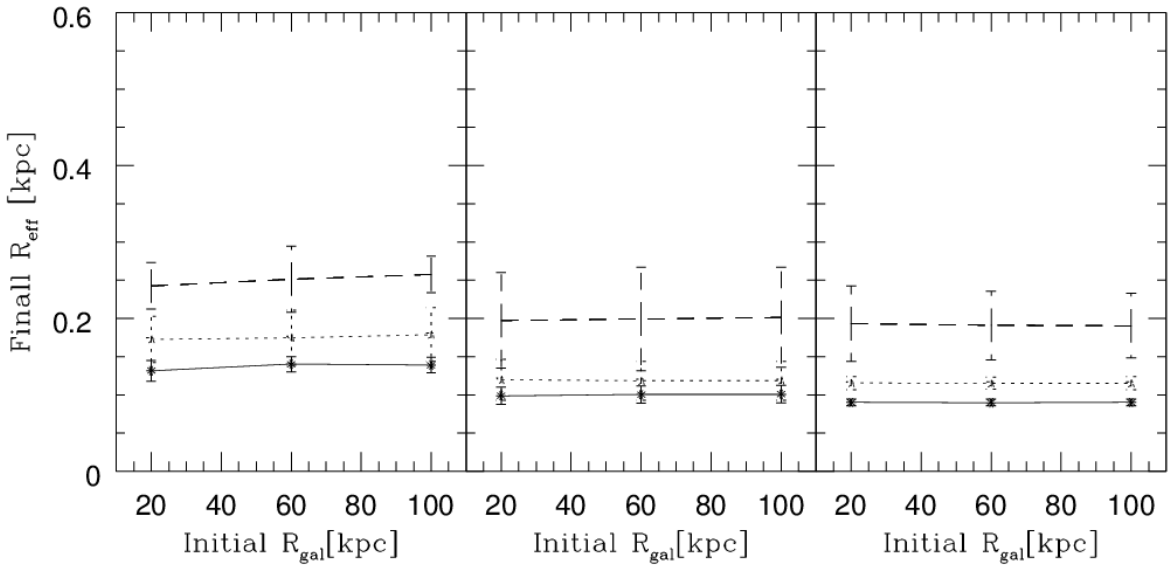

Figure 5.7: Resulting effective radii as function of the galactic distance. The 3 panels show from left to right the results for SC/UCD with R_{sc}=4, 10 and 20 pc, respectively. In each panel the solid line is associated with CC radii of R_{cc} = 50 pc, the dotted line represents R_{cc} = 100 pc and the dashed line R_{cc} = 200 pc. The data point are mean values calculated from 3 realizations of these parameters with the associated 1 σ deviation as error-bars. Source: From this work.

For 5.8 and 5.9 we now use mean values obtained from making all simulations with the same

R_{sc} and R_{cc} together independent of their galactic distance. In Fig 5.8 you can see the behavior of the R_{eff} as function of the initial size of the SCs/UCDs R_{sc}. The label of the lines is the same as Fig 5.7. It is possible to see that the R_{eff} and the R_{cc} are proportional. And also it is possible to see according to the different lines that bigger values of R_{sc} give us a smaller value for R_{eff}, because of the increasing of the filling factor as is explained in Section 5.1. So we claim that the effective radius of the final object depends inversely proportional with the initial size of the SCs/UCDs.

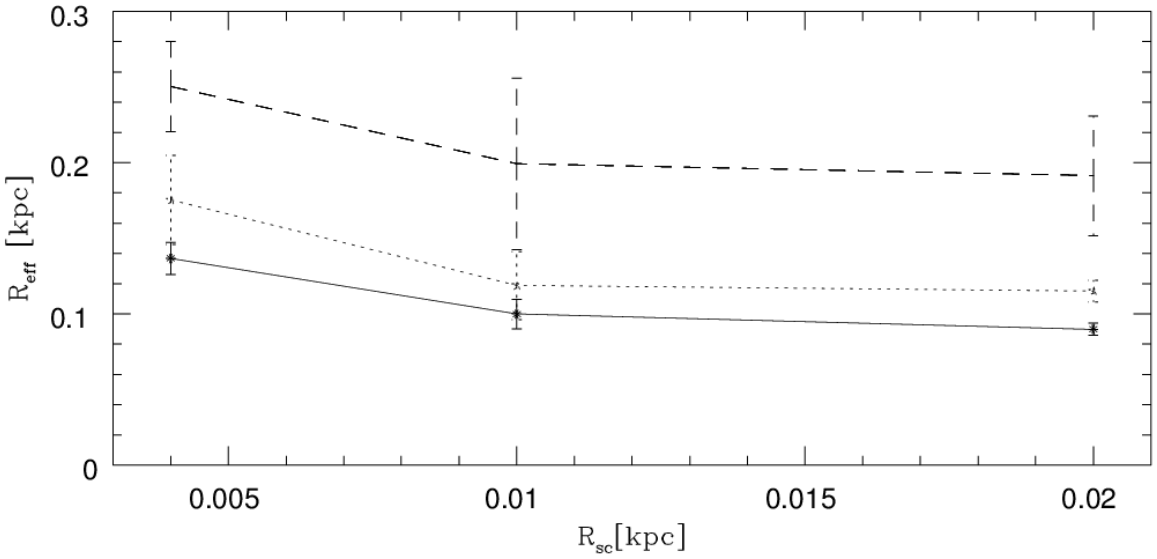

Figure 5.8: Behavior of the R_{eff} as function of the initial size of the SCs/UCDs R_{sc}. The label of the lines is the same of 5.7.In this plot we use all simulations with the same parameters but independent of the distance to the galaxy, so 9 values to calculate mean and errors. Source: From this work.

Fig 5.9 displays the behavior of the R_{eff} as function of the initial size of the distribution R_{cc}. If we see Fig 5.8 the results for 10 and 20 pc are the same so we do the average of the all simulations with sizes of SCs/UCDs of 10 and 20 pc, so 18 values to calculate the mean and errors. The different lines represent different sizes of the SCs/UCDs, the big dashed line is associated with R_{sc}=4 pc , the point-dashed line with R_{sc}=10 and 20 pc. Also a linear fit is shown in red and blue for the big dashed line and the point-dashed line respectively:

$$f(R_{sc}) = a \times R_{sc} + b \tag{5.1}$$

The values of a and b are the following:

- For the big dashed line
  a= 0.755±0.006
  b= 0.0993±0.0008

- For the point-dashed line:
  a= 0.69±0.08
  b= 0.06 ±0.01

So, we could write:

$$R_{eff} \sim 0.7 R_{cc} \tag{5.2}$$

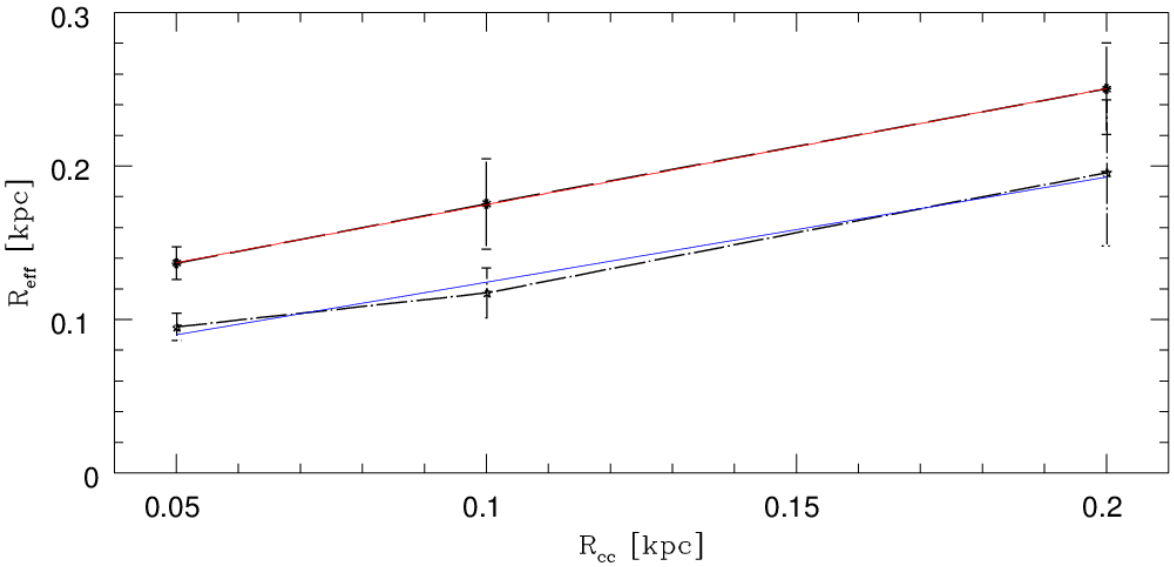

Figure 5.9: Behavior of the R_{eff} as function of the initial size of the CC R_{cc}. The different lines represent different sizes of the SCs/UCDs, the big dashed line is associated with R_{sc}=4 pc , the point-dashed line with R_{sc}=10 and 20 pc. In this plot for the big dashed line we use all simulations with the same parameters but independent of the distance to the galaxy, so 9 values to calculate mean and errors, but for the the point-dashed line we do the average of the all simulations with sizes of SCs/UCDs of 10 and 20 pc, so 18 values to calculate the mean and errors. Also a lineal fit is shown in red and blue for the big dashed line and the point-dashed line respectively. Source: From this work.

Again, we see a dependence on the chosen scale-length of the CC distribution, i.e. the larger the Plummer radius of the CC, the larger the effective radius of the final cE. And a bigger value of R_{sc} give us a smaller value for R_{eff}, because of the increasing of the filling factor as is explained in Section 5.1.

If we consider an R_{eff} value for a compact elliptical between 80 pc and 200 pc, only the simulations where the initial size of the SCs/UCDs is 4 pc and the size of the CC is 200 pc do not end up having merger object within that range (see Fig5.8).

It looks like the results are indeed linear proportional to R_{cc} as we show in Fig 5.9. But we also see that only the R_{sc}=4 pc results differ. R_{sc}=10 pc and R_{sc}=20 pc are very similar and closer to what we want as cE. So considering the sizes of the initial objects in the simulation it is more likely that the merging of UCDs produce cEs than merging SC (at least for R_{eff}).

5.2.1 Filling Factor. α parameter as function of R_{eff}

In Fig 5.10 you can see how the effective radius of the final object depends on the α parameter which is defined as:

$$\alpha = \frac{R_{sc}}{R_{cc}} \tag{5.3}$$

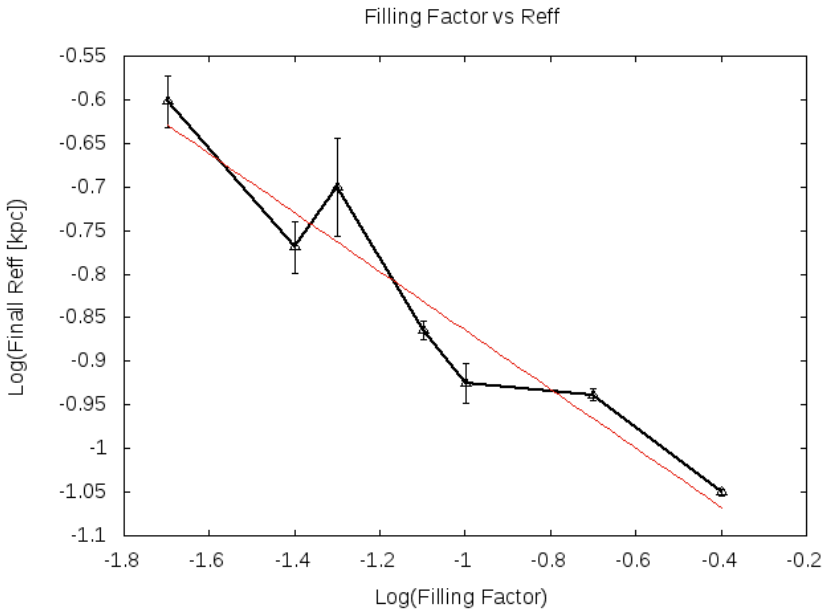

Figure 5.10: Effective radius of the final object against the α parameter. This figure was made taking the values of the average of the simulation with different values of distance to the center of the galaxy. Also a fit is shown in red. Source: From this work.

For the data points in Fig 5.10 we use all simulations with the same filling factor independent of their distance to the galaxy.
The effective radius of the final object increases when we decrease the α parameter.
The filling factor is inversely proportional with the effective radius of the final object. This is totally expected because the filling factor tells us how dense the system is, and denser initial distributions of objects lead to denser final merger objects.
Also a fit is shown in red. The fit follow :

$$R_{\text{eff}} = A \times \alpha^{B} \tag{5.4}$$

The values of a and b are the following:
A=-1.20 $\pm$ 0.05
B=-0.34 $\pm$ 0.05
So, we could write:

$$\mathrm{R_{eff}} \sim \alpha^{-1/3} \tag{5.5}$$

5.3 Surface Brightness(Σ_0)

In this section we present the central surface brightness(Σ_0) of all 81 simulations.
The data points for the Σ_0 are obtained with IDL which gives us the Σ_0 profiles integrated light along a line of sight as is explained in Chapter 4. Then we calculate a mean value out of three possible line of sight along Cartesian coordinates axis x, y and z. In this section we consider the value for the central section of the final object. The mean value Σ_0 was obtained with the results of the average of three different initial distributions of the SC in the CC. And the error was obtained with the standard deviation of these three values.

In Fig 5.11 we show the central surface brightness of the final object as function of the galactic distance. The 3 panels show from left to right the results for SC/UCD with R_{sc}=4, 10 and 20 pc, respectively. In each panel the solid line is associated with CC radii of $R_{cc} = 50$ pc, the dotted line represents $R_{cc} = 100$ pc and the dashed line $R_{cc} = 200$ pc. The data point are mean values calculated from 3 realizations of these parameters with the associated 1 σ deviation as error-bars.
As a result we see almost horizontal lines, i.e. the central surface brightness does not depend on the distance of the CC to the galactic center.

If we increase the initial Plummer radius of the distribution we obtain a fainter value for the central surface brightness. So, the central surface brightness of the final object is proportional with the Plummer radius of the distribution.

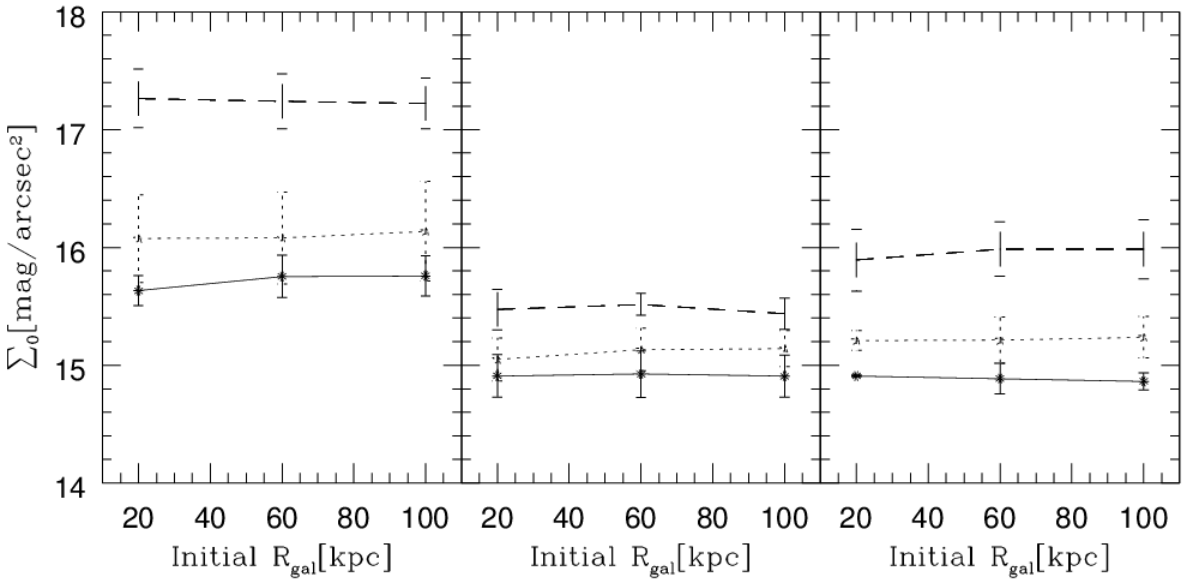

Figure 5.11: Final central surface brightness as function of the galactic distance. The 3 panels show from left to right the results for SC/UCD with R_{sc}=4, 10 and 20 pc, respectively. In each panel the solid line is associated with CC radii of R_{cc} = 50 pc, the dotted line represents R_{cc} = 100 pc and the dashed line R_{cc} = 200 pc. The data point are mean values calculated from 3 realizations of these parameters with the associated 1 σ deviation as error-bars. Source: From this work.

In Fig 5.12 and Fig 5.13 we use all simulations with the same parameters but independent of the distance to the galaxy.

Fig 5.12 show the behavior of the central surface brightness of the final object given in mag arcsec^{-2} using a mass-to-light ratio of 1 to convert our simulations values, measuring mass per area as function of the initial R_{sc}. Here, the label of the lines is the same of 5.11.

It is possible to see that while we increase the size of the SCs/UCDs we obtain a fainter value for the central surface brightness except the simulations where the initial size of the SCs/UCDs is R_{sc}=4 pc, in this case we already explained in the previous section that the final object is ruled out of resembling a cE, because of the mass, (the number SCs/UCDs in the final object is too small), this leads to a very small luminosity (big value of of central surface brightness mag/arcsec^2) of the final object compared to all the other simulations we are analyzing.

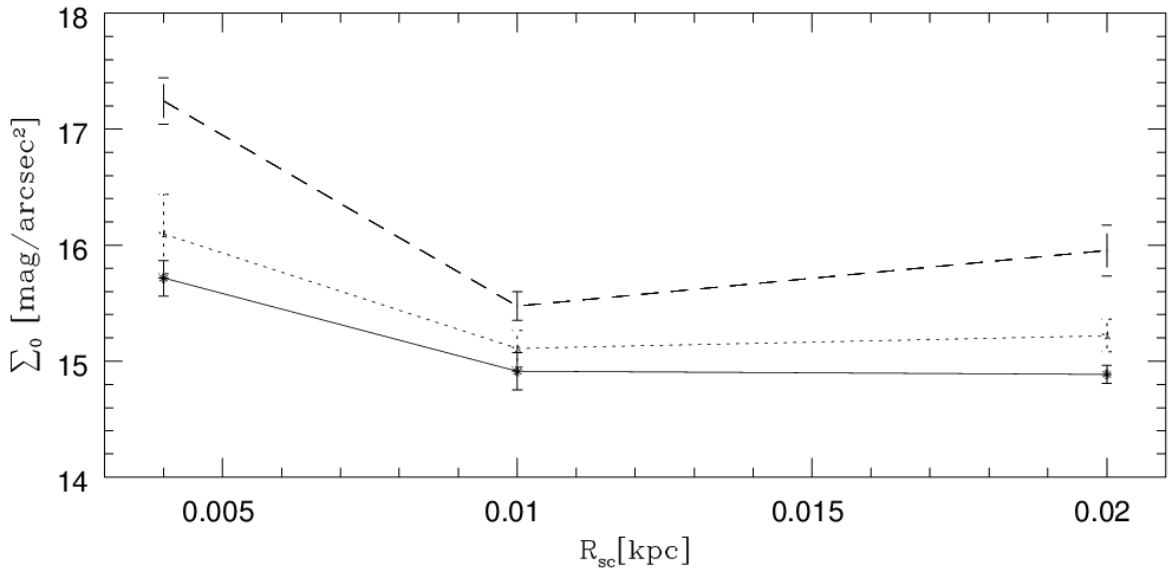

Figure 5.12: Behavior of the Σ_0 as function of the initial size of the SCs/UCDs R_{sc}. The label of the lines is the same of 5.11.In this plot we use all simulations with the same parameters but independent of the distance to the galaxy, so 9 values to calculate mean and errors. Source: From this work.

This is consistent with Fig 5.13 were we show the behavior of the central surface brightness . Different lines represent different sizes of the SCs/UCDs, the big dashed line is associated with R_{sc}=4 pc , the point-dashed line with R_{sc}=10 pc and the small-large dashed line with R_{sc}=20 pc.
Also a lineal fit is shown in red, green and blue for the big dashed line, point-dashed line and small-large dashed line, respectively. The fit follow a linear fit :

$$f(R_{cc}) = a \times R_{cc} + b \tag{5.6}$$

The values of a and b are the following:

- For the big dashed line
  a= 10.4±0.9
  b= 15.1±0.1
- For the point-dashed line:
  a= 3.74±0.05
  b= 14.729±0.007
- For the small-large dashed line:
  a= 7.2±0.2
  b= 14.52±0.02

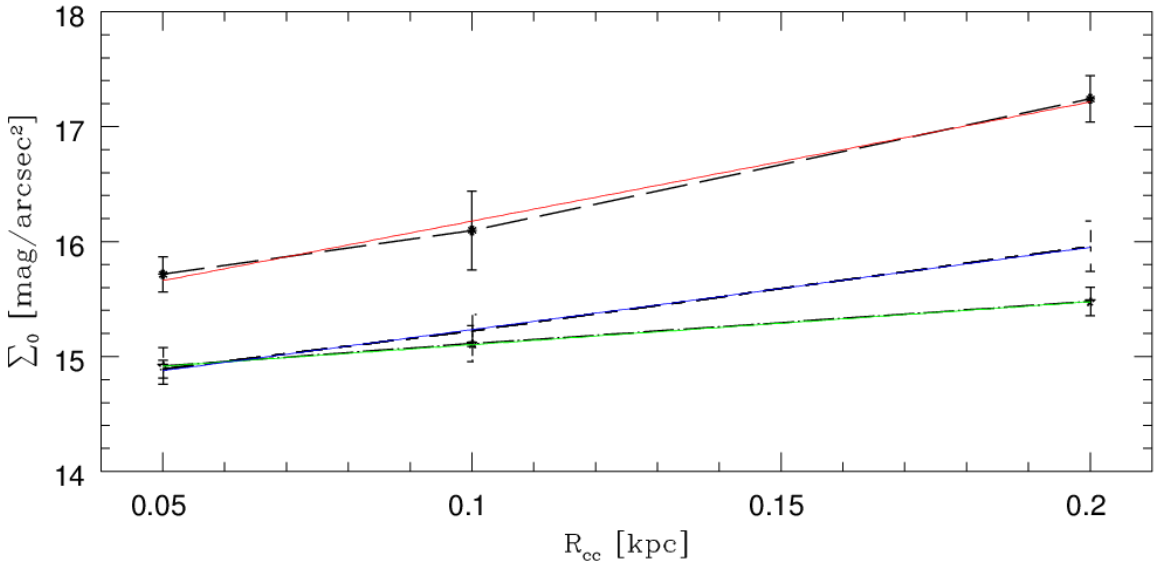

Figure 5.13: Behavior of the Σ_0 as function of the initial size of the SCs/UCDs R_{cc}. The different lines represent different sizes of the SCs/UCDs, the big dashed line is associated with R_{sc}=4 pc , the point-dashed line with R_{sc}=10 and the small-large dashed line with R_{sc}=20 pc. In this plot we use all simulations with the same parameters but independent of the distance to the galaxy, so 9 values to calculate mean and errors.Also a lineal fit is shown in red, blue and green for the big dashed line, point-dahed line and small-large dashed line, respectively. Source: From this work.

The surface brightness of known cE goes approximately from 14 to 20 mag (see table 1 of Chilingarian et al 2007, table 2 of Huxor et al 2013 and references therein). Considering this range of Σ_0 every simulation in our work reproduces well the values for cEs.

5.3.1 Filling Factor. α parameter as function of Σ_0

In figure 5.14 you can see how the central surface brightness of the final object depends on the α parameter. In this plot we use all simulations with the same parameters but independent of the galactic distance. We can see that the Σ_0 and the filling factor are inversely proportional following a power law, which means, when we increase the filling factor we obtain brighter objects -smaller values for the central surface brightness-.

Also a power law fit is shown in light blue. The fit follows :

$$\Sigma_0 = A \times \alpha^B \tag{5.7}$$

The values of a and b are the following:
A=13.9±0.4
B=-0.05±0.01

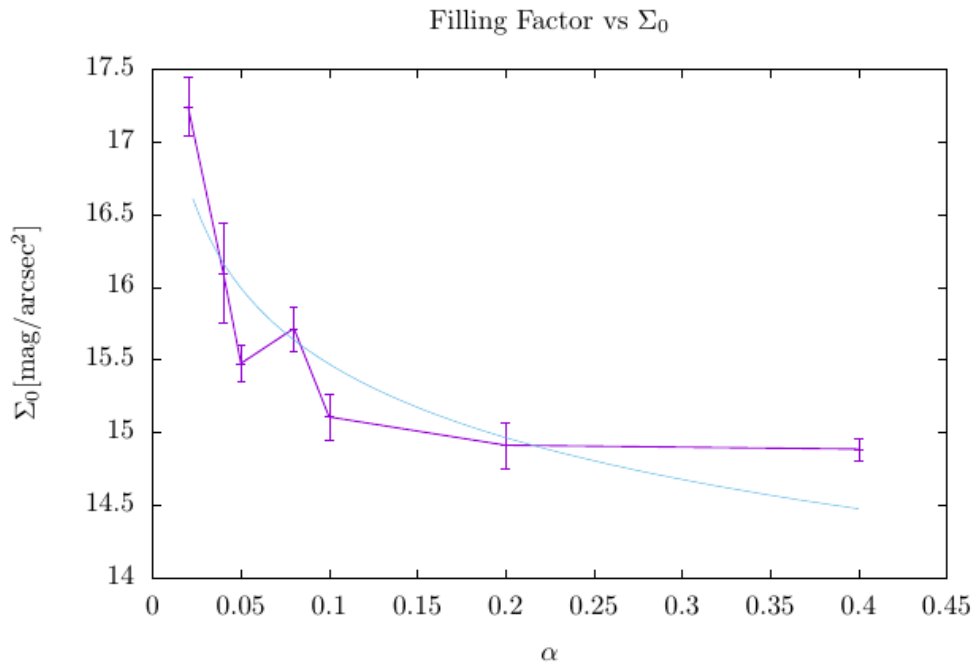

Figure 5.14: Central surface brightness of the final object against the α parameter. This figure was made taking the values of the average of the simulation with different values of distance to the center of the galaxy. Also a power law fit is shown in light blue. Source: From this work.

This is expected because the filling factor is how densely the system is filled with SCs/UCDs, so simulations with high α will end in a compact object, and simulations with low α in extended object.

5.4 Shapes

5.4.1 Ellipticity

The ellipticity of an object is defined by

$$\epsilon = 1 - \frac{b}{a}$$

where a and b are the semi-major and minor axis of an ellipse, respectively. The ellipticity is obtained from IRAF. In IRAF we use the ELLIPSE routine, from where we can obtain the ellipticity value at different radii for each isophote, The chosen value for the radius of the isophote, for the analysis the ellipticity is approximately 100 pc.

In the literature it is usually considered that compact ellipticals have no significant ellipticity (e.g Igor Chilingarian and Ivan Zolotukhin (2015)). The ellipticity of M32 is about E2 which means that the smaller axis is about 20% shorter than its larges axis (Batcheldor et al 2013). The exact ellipticity of M32 is 0.17 (Kent 1987).

The ellipticity of the final object seems not to follow a clear trend according to plots in function as R_{gal}, R_{sc} and R_{cc}, like the previous sections. But in Fig 5.15 one can see that almost all the simulations have ellipticities in the range of cEs, i.e. ϵ=0.2 or less.

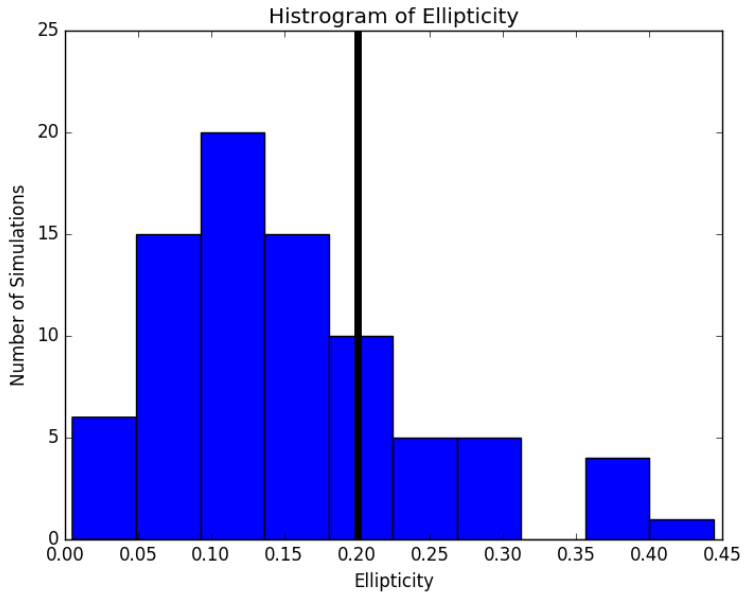

Figure 5.15: Histogram with the ellipticities of the final object. Most of the simulations have a ellipticity in the range of cEs. There is a black line on ϵ=0.2. Source: From this work.

5.5 Velocity Dispersion(σ_0)

In this section we present the central velocity dispersion of all 81 simulations.
The velocity dispersion is the standard deviation for the mean velocity of the particles in the object. In this section we compare the central velocity dispersion of the final objects.
We obtain the data-points for the velocity dispersion from the IDL script as it is explained in Chapter 4. We take the average of the three data points that are asociated with the three lines of sight x, y and z.

In Fig 5.16 we show the central velocity dispersion of the final object as function of the galactic distance. The 3 panels show from left to right the results for SC/UCD with R_{sc}=4, 10 and 20 pc, respectively. In each panel the solid line is associated with CC radii of R_{cc} = 50 pc, the dotted line represents R_{cc} = 100 pc and the dashed line R_{cc} = 200 pc. The data point are mean values calculated from 3 realizations of these parameters with the associated 1 σ deviation as error-bars.
As a result we see almost horizontal lines, i.e. the central velocity dispersion just as R_{eff} and central surface brightness of the final object does not depend on the initial distance of the CC to the galactic center.

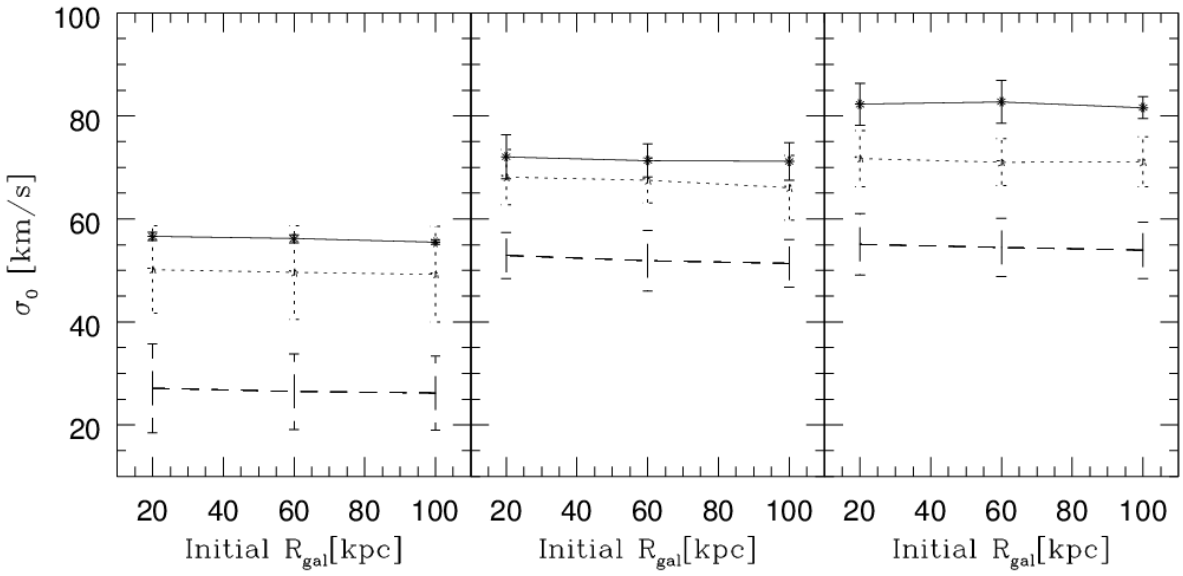

Figure 5.16: Final central velocity dispersion as function of the galactic distance. The 3 panels show from left to right the results for SC/UCD with R_{sc}=4, 10 and 20 pc, respectively. In each panel the solid line is associated with CC radii of R_{cc} = 50 pc, the dotted line represents R_{cc} = 100 pc and the dashed line R_{cc} = 200 pc. The data point are mean values calculated from 3 realizations of these parameters with the associated 1 σ deviation as error-bars. Source: From this work.

In Fig 5.17 and Fig 5.18 we use all simulations with the same parameters but independent of the distance to the galaxy.

In 5.17 the behavior of the σ_0 as function of the initial size of the SCs/UCDs R_{sc} is displayed. The label of the lines of this plot is the same of 5.16. It is possible to see, that while we increase the initial Plummer radius of the single SCs or UCDs we obtain a bigger σ_0 for the final object. So we claim that the central velocity dispersion of the final object is proportional to the initial radius of the SCs/UCDs.

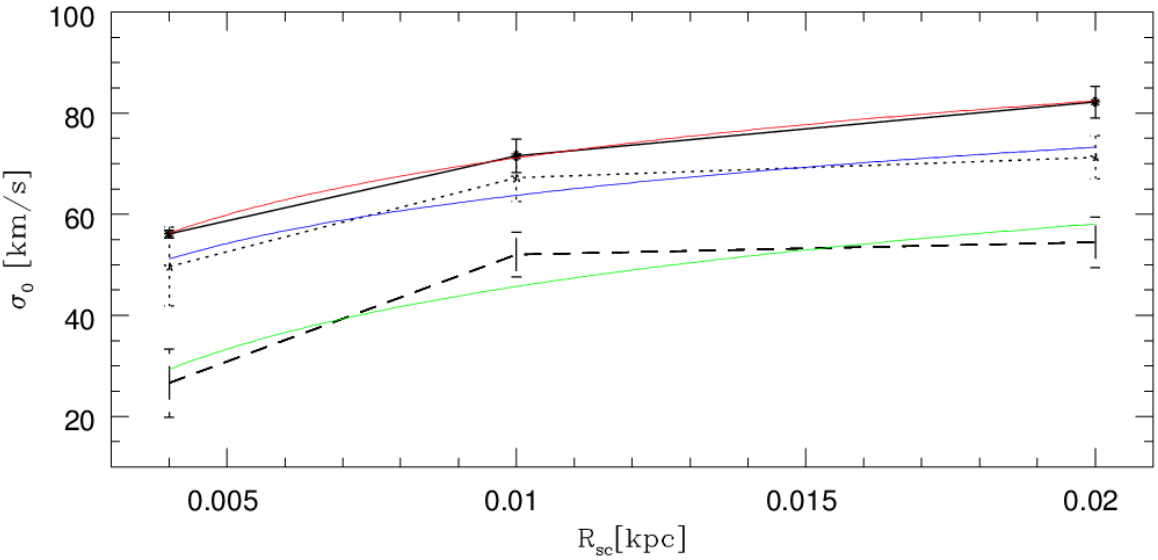

Figure 5.17: Behavior of the σ_0 as function of the initial size of the SCs/UCDs R_{sc}. The label of the lines is the same of 5.16.Also a fit of a logarithmic function is shown in red for the solid line, blue for the dotted line and green the dashed line. In this plot we use all simulations with the same parameters but independent of the distance to the galaxy, so 9 values to calculate mean and errors. Source: From this work.

Also a fit of a logarithmic function is shown in red for the solid line, blue for the dotted line and green the dashed line. The fit of logarithmic function:

$$f(R_{sc}) = a \times log(R_{sc}) + b \tag{5.8}$$

The values of a and b are the following:

- For the solid line
  a= 37.4±0.9
  b= 146 ±2
- For the dotted line:
  a= 32±9
  b= 127 ±18

- For dashed line:
  a= 41±16
  b= 128±32

Also it is possible to see that while we increase the initial Plummer radius of the distribution we obtain a smaller σ_0. So σ_0 and R_{cc} are inversely proportional, this is easy to see in Fig 5.18. Fig 5.18 show the behavior of σ_0 as function of the initial size of the distribution R_{cc} Different lines represent different sizes of the SCs/UCDs, the big dashed line is associated with R_{sc}=4 pc , the point-dashed line with R_{sc}=10 pc and the small-large dashed line with R_{sc}=20 pc.

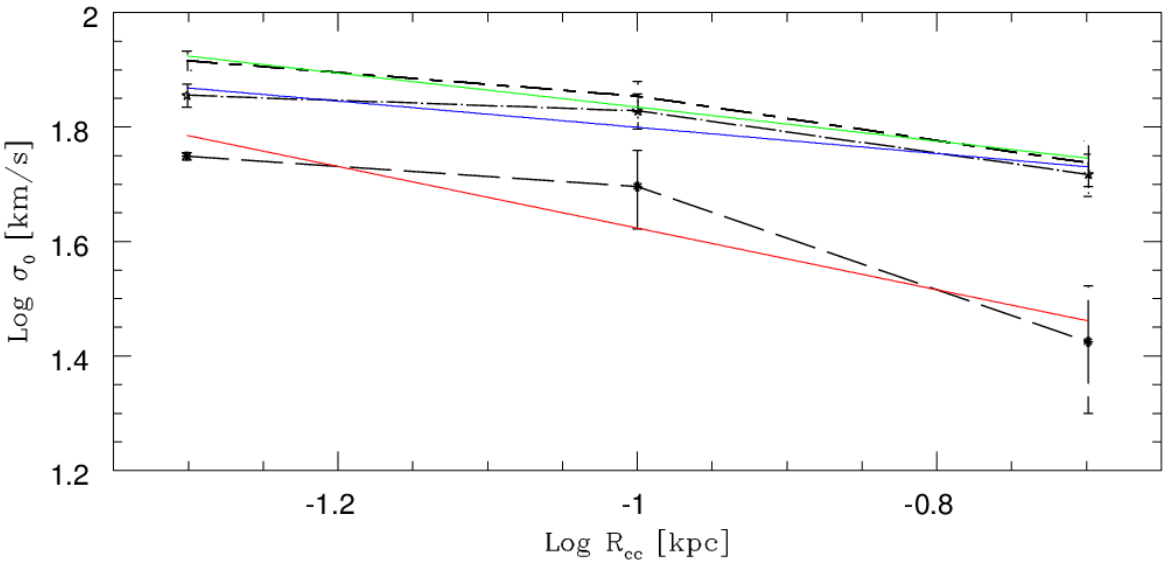

Figure 5.18: Behavior of the σ_0 as function of the initial size of the SCs/UCDs R_{cc}. The different lines represent different sizes of the SCs/UCDs, the big dashed line is associated with R_{sc}=4 pc , the point-dashed line with R_{sc}=10 and the small-large dashed line with R_{sc}=20 pc. In this plot we use all simulations with the same parameters but independent of the distance to the galaxy, so 9 values to calculate mean and errors. Also a fit is shown in red, blue and green for the big dashed line, point-dahed line and small-large dashed line, respectively. Source: From this work.

Also a fit is shown in red, blue and green for the big dashed line, point-dashed line and small-large dashed line, respectively. The fit follow a lineal fit :

$$f(R_{cc}) = a \times R_{cc}^{b} \tag{5.9}$$

The values of a and b are the following:

- For the big dashed line
  a= 12.2±1.6
  b= -0.5 ±0.2
- For the point-dashed line:
  a= 37.2±1.2
  b= -0.23 ±0.08
- For the small-large dashed line:
  a= 34.5±1.1
  b= -0.30±0.05

So, we could write:

$$\sigma \sim \mathrm{R}_{\mathrm{cc}}^{-0.5} \tag{5.10}$$

This is directly related with the virial theorem in where :

$$\langle \sigma^2 \rangle = \frac{GM}{r_g} \tag{5.11}$$

where r_g is the gravitational radius. So it is possible to see that the velocity dispersion is proportional with the mass of the system, but inversely proportional with the radius of the distribution. This is easy to see in Fig 5.18 and Fig 5.17.

The range of central velocities dispersion that have cE is huge, could be from a few tens km/s, for example NGC2970 (47.7 ± 1.6) until a couple of hundred km/s like PSC012519 (222.2 ± 2.3). (see table 2 of Anna Ferré-Mateu et al 2017.)
The central velocity dispersion of M32 is 76 ± 10 km/s (van der Marel et al. 1998).
If we consider a central velocity dispersion of at least 40 km/s for cE, only the simulations where the initial size of the SCs/UCDs is 4 pc and the size of the CC is 200 pc does not fit in this range.

5.5.1 Filling Factor. α parameter as function of σ_0

In figure 5.19 you can see how the central surface brightness of the final object depends on the α parameter. In this plot we use all simulations with the same parameters but independent of the galactic distance. We can see that the σ_0 and the Filling factor are proportional.

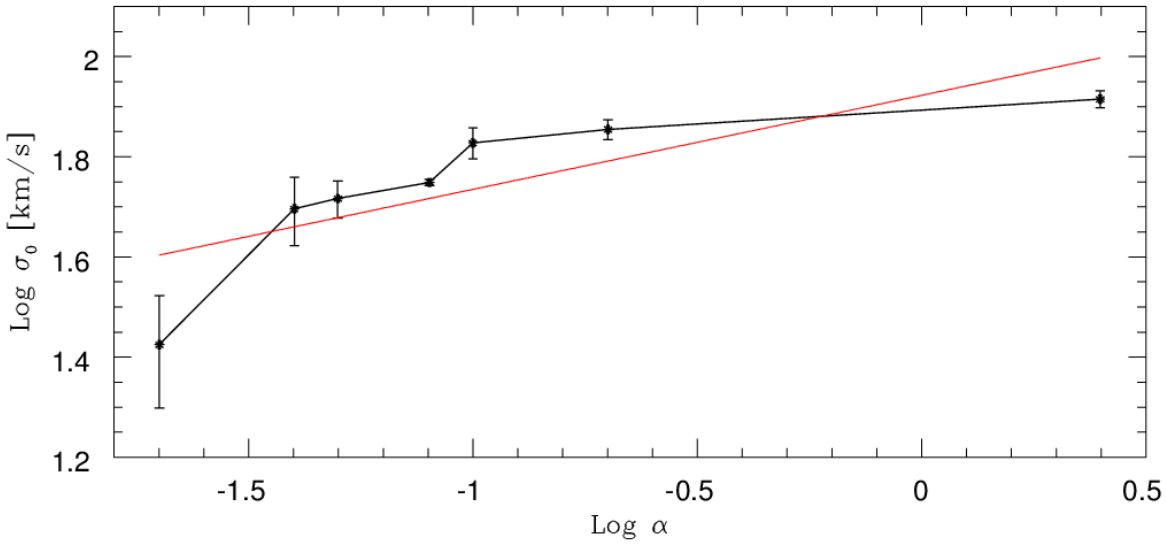

Figure 5.19: Velocity dispersion of the final object against the α parameter. This figure was made taking the values of the average of the simulation with differents values of distance to the center of the galaxy. Also a power law fit is shown in light blue. Source: From this work.

Also a power law fit is shown in light blue. The fit follow :

$$\sigma_0 = A \times \alpha^B \tag{5.12}$$

The values of a and b are the following:
A=83.7±1.2
B=0.19 ±0.06

So we could right the following relation:

$$\sigma_0 \sim \alpha^{0.2} \tag{5.13}$$

Chapter 6

Simulation of cE with 128 UCDs

In this chapter we present one special simulation with initial number of UCDs of N_0^{cc}=128. This simulation has a size of the CC of R_{cc}= 100 pc, an initial size of the UCDs of R_{sc}= 20 pc and a initial distance to the center of the galaxy of R_{gal}=100 kpc. The final object is the result of the merging of 128 UCDs corresponding to $\sim 10^9$ $M_\odot$.

We present in Fig 6.1 the contour map of the final object until a radius of 1.5 kpc. Fig 6.1 is the shape of the final object with a color bar for the magnitude of the surface brightness. The ellipticity of this object is 0.130±0.001 while the ellipticity of M32 is 0.17 (Kent 1987).

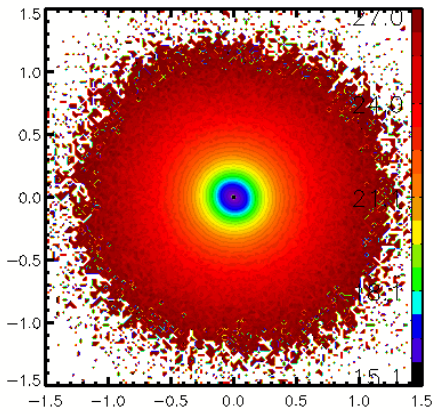

Figure 6.1: Characteristics of the final object until a radius of 1.5 kpc. We show the shape of the final object with a color bar for the magnitude of the surface brightness. Source: From this work.

Fig 6.2 is a plot of the radial profile of the surface brightness. The central surface brightness of this object is Σ= 15.13 mag/arcsec^2 using a generic M/L ratio of 1. The central bulge surface brightness of M32 is 15.31 R mag/arcsec^2(Graham, 2002).

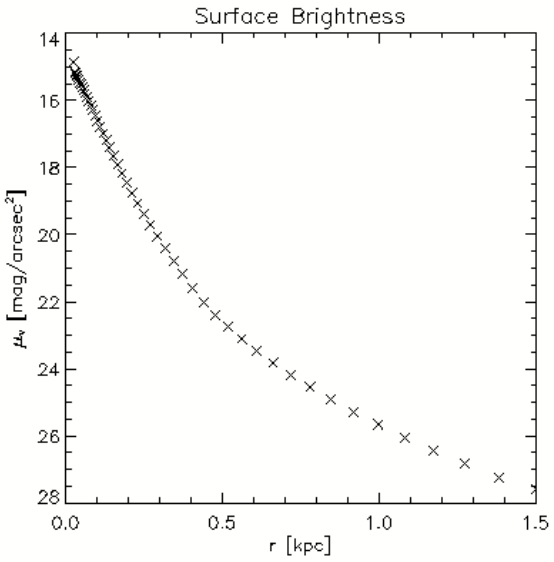

Figure 6.2: Radial profile of the surface brightness of the final object. Source: From this work.

In Fig 6.4 is shown the surface brightness in $M_\odot/pc^2$, and a fit with a Sersic profile to obtain the R_{eff}. This gives us a value of R_{eff}=101±8 pc while the effective radius of M32 is ∼ 29" (Choi et al. 2002). The values for the fit of 6.4 are the following:
I_e= 9000±1000[$M_\odot/pc^2$]
R_e= 0.101±8 pc
n = 1.2±0.1

Fig 6.4 is a plot of the radial profile of the velocity dispersion. The central velocity dispersion of this object is σ= 80.3 km/s. The central velocity dispersion of M32 is 76 ± 10 km/s (van der Marel et al. 1998).

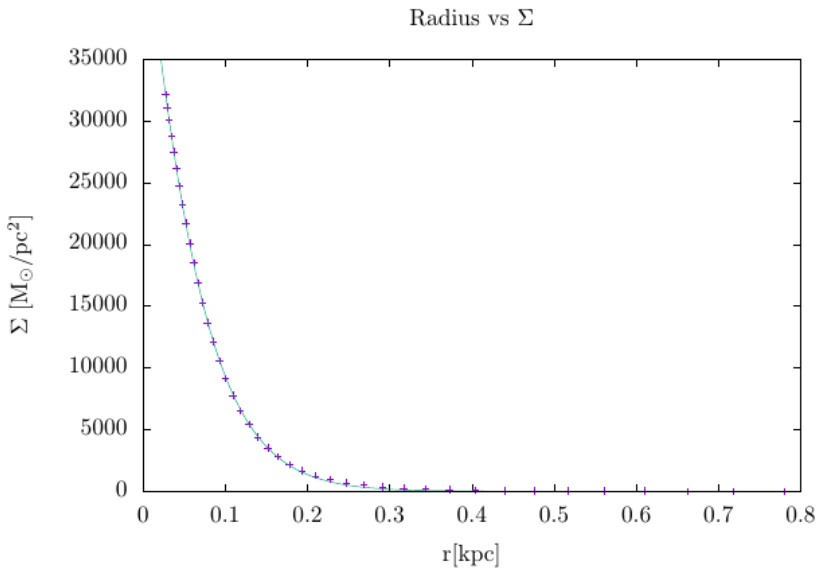

Figure 6.3: Surface brightness in $M_{\odot}/pc^2$, and a fit with a Sersic profile to obtain the R_{eff}. Source: From this work.

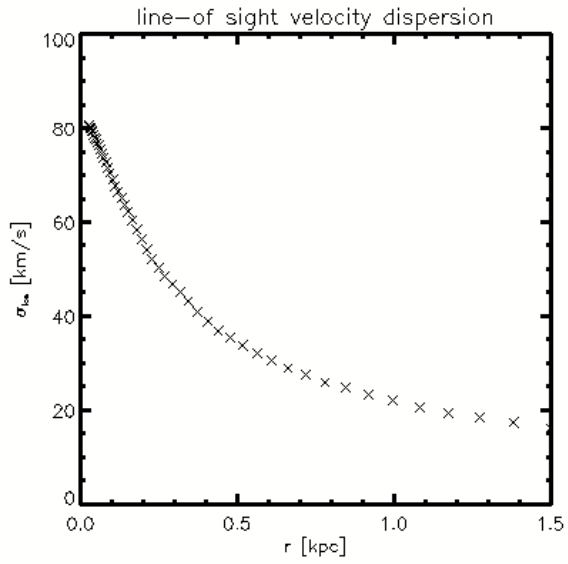

Figure 6.4: Radial profile of the velocity dispersion of the final object. Source: From this work.

All characteristic of the final object shown in this Chapter are very similar to the observed characteristics of M32, and are evidently in the range of the values of all known cE.

Chapter 7

Discussion and Conclusions

Every simulation performed in this work leads through the merging star cluster scenario, to a final stable object with characteristics of EC, FF and UCDs in Chapter 4 and of cE in Chapter 5 and 6. The results of our models with 64 SCs/UCDs (Chapter 5) to reproduce a cE, tell us:

- The analysis of the final mass, shape, R_{eff}, Σ and σ show that cE form from UCDs rather than SCs. This is directly related with the Filling factor α, simulations with bigger α have more SCs/UCDs that merge, on the other hand the low α gives us a small number of SCs/UCDs in the final object, this is because the Filling factor tells us how densely the system is filled with SCs/UCDs.

- The R_{eff} is in the range of 90 and 260 pc which is consistent with the sizes of cEs. Also, with the fitting lines we obtain, using a sersic-fit, the relation: $R_{eff} \approx 0.7 R_{cc}$.

- The range of ϵ is between 0.05 and 0.32, but almost all simulations are in the range of cE (ϵ=0.2 or less).

- The Σ_0 of our models is in the range of 15 and 17.5 mag/arcsec^2, so all simulations fit in the range of the Σ_0 of cEs.

- Most of the results of the simulations show a σ_0 between ∼50 and ∼80 km/s, which are in the range of σ_0 of cE. Only 3 sets of initial parameters lead to an object with σ_0 smaller than this range. This 3 simulations were already discarded to be a cE because of the final mass of the system. Also, with the fitting lines we probe the relation coming from the virial theorem, between σ_0 and R_{cc} : $\sigma_0 \approx R_{cc}^{-0.5}$.

There are some disadvantages, or behaviors that we can not reproduce in this simulations, like the star formation history (SFH). Two main dominant populations are detected in M32 by Monachesi et al. 2012(see Monachesi et al. 2012):

1. $\sim$ 40%±17% of the mass in a 2–5 Gyr old, metal-rich population ([M/H] = 0.02 ± 0.01 dex).

2. $\sim 55\% \pm 21\%$ of the total mass in stars older than 5 Gyr, with slightly subsolar metallicities.

Also our simulations can not treat metalicities, we perform simulations that treat only dynamics of the particles. The mass-weighted mean age of M32 is: $\langle \text{Age} \rangle = 6.8 \pm 1.5$ Gyr and its mass-weighted mean metallicity $\langle [\text{M/H}] \rangle = 0.1 \pm 0.08$ dex. (see Monachesi et al. 2012).

But in Alarcon et al 2018, a similar scenario in where SCs are dissolved to form a dSph is studied, but in a dark matter halo. In this work different SFH are applied. The different SFH do not show a big difference between the results, so taking this result we could consider that in our work even if we add a SFH to the models, the results won't be so different than the results shown in this work.

The merging star cluster scenario may not be the only way to produce a cE; maybe more scenarios are true, like the tidal stripping and truncation scenario (Faber 1973), either with an origin of an elliptical galaxy truncated with a dense core (e.g King 1962; Faber 1973) or be a bulge of a partially stripped disk galaxy (e.g Bekki et al. 2001) Or cEs could also have an intrinsic origin due the natural extension of the class of elliptical galaxies to smaller sizes and lower luminosities (Wirth & Gallagher 1984; Kormendy et al. 2009).

But our models reproduce very well the dynamical properties of cEs and may therefore be a valid formation channel, so the merging star cluster scenario is able to produce objects with characteristics of EC, FF, UCDs and cE, depending in the total mass of the system and the object in the cluster complex (SCs or UCDs).

Chapter 8

Bibliography

Alarcón Jara, A. G., Fellhauer, M., Matus Carrillo, D. R., Assmann, P., Urrutia Zapata, F., Hazeldine, J., Aravena, C. A.,2018, MNRAS, 473, 5015

Barmby,P., Huchra, J.P., 2001, AJ, 121, 1482

Bastian, N., Gieles, M., Efremov, Y. N., Lamers, H. J. G. L. M. 2005, A&A, 443, 79

Bastian, N., Schweizer, F., Goudfrooij, P., Larsen, S. S., Kissler-Patig, M. 2013, MNRAS, 431, 1252

Bekki K., Couch W. J., Drinkwater M. J., Gregg M. D., 2001, ApJ, 557, L39

Bill Keel's image collection at the University of Alabama.

Brodie, J. P., Larsen S. S. 2002 AJ, 124, 1410

Brüns, R. C., Kroupa, P., Fellhauer, M. 2009, ApJ, 702, 1268

Brüns, R. C., Kroupa, P. 2011, ApJ, 729, 69

Brüns, R. C., Kroupa, P., Fellhauer, M., Metz, M., & Assmann, P. 2011, A&A, 529, 138

Brüns, R. C., Kroupa, P. 2012, A&A, 547, 65

Brüns 2013 PhD thesis, University of Bonn.

Bruzual, G., Charlot, S., 2003, MNRAS, 344, 1000

Burkert, A., Brodie, J., Larsen, S. 2005, AJ, 628, 231

Catalog of Messier 1850

Chies-Santos,A. L., Santiago, B. X., Pastoriza, M. G., 2007, A&A, 467, 1003

Chilingarian, I., 2007, A&A, 466, L21 Choi, P. I., Guhathakurta, P., Johnston, K. V. 2002, AJ, 124, 310 Drinkwater, M. J., Jones, J. B., Gregg, M. D., Phillipps, S. 2000, PASA, 17, 227

Drinkwater M., J, 2004, PASA, 21, 375

Evstigneeva, E. A., Drinkwater, M. J., Peng, C. Y., et al. 2008, AJ, 136, 461

Evstigneeva, E. A., Gregg, M. D., Drinkwater, M. J., Hilker, M. 2007, AJ, 133, 1722

Faber S. M., 1973, ApJ, 179, 423

Fellhauer M., Baumgardt H., Kroupa P., Spurzem R., 2002, CeMDA, 82, 113

Fellhauer M., Kroupa P., Baumgardt H., Bien R., Boily C. M., Spurzem R., Wassmer N., 2000,

New Astron., 5, 305
Fellhauer, M., Kroupa, P., 2002a, MNRAS, 330, 642
Fellhauer, M., Kroupa, P. 2002b, AJ, 124, 2006
Fellhauer, M., Kroupa, P., 2005, MNRAS, 359, 223
Ferré-Mateu,A., Forbes, D. A., Romanowsky, A. J., Janz, J., Dixon, C. 2017, MNRAS, 473, 1819
Forbes D. A. et al 2013 , MNRAS, 435
Graham D. A., 2002, ApJ, 568, L13
Hasegan, M., Jordán, A., Coté, P., et al. 2005, ApJ, 627, 203
Harris, W. E. 1991, ARA&A, 29, 543
Harris, W.E. 1996 Globular Cluster Systems list, McMaster University
Hilker, M., Infante, L., Vieira, G., Kissler-Patig, M., Richtler, T. 1999, A&AS, 134, 75
Huxor A. P., Phillipps S., Price J., Harniman R., 2011, MNRAS, 414, 3557
Huxor,A. P., Phillipps,S. , Price, J., 2013, MNRAS, 430, 1956
Hwang, N., Lee, M. G., Lee, J. C., et al. 2011, ApJ, 738, 58
Janz J. et al., 2016, MNRAS, 456, 617
King, I. 1962, AJ, 67, 471
Kissler-Patig, M. 2004, in Astronomical Society of the Pacific Conference Series, Vol. 322, The Formation and Evolution of Massive Young Star Clusters, ed. H. J. G. L. M. Lamers, L. J. Smith, A. Nota, 535
Kormendy, J., Bender, R., 2012, ApJS, 198, 2 Kormendy, J., Fisher, D. B., Cornell, M. E., Bender, R., 2009, ApJS, 182, 216
Kroupa, P.,1998 , MNRAS, 300, 200
Larsen, Brodie, 2000, AJ, 120, 2938
Lee, M. G., Chandar, R., Whitmore, B. C. 2005, AJ, 130, 2128
Maraston, C., Bastian, N., Saglia, R. P., et al. 2004, A&A, 416, 467
Mieske, S., Hilker, M., Infante, L., 2002, A&A, 383, 823
Mieske, S., Hilker, M., Jordán, A., et al. 2008, A&A, 487, 921
Monachesi, A., Trager, S. C., Lauer, T. R., et al. 2012, ApJ, 745, 97
Norris, M. A., Kannappan, S. J., 2011, MNRAS, 414, 739
Plummer, H. C., 1911, MNRAS, 71, 460
Pryor, C., Meylan, G. 1993, in ASP Conf. Ser. 50, Structure and Dynamics of Globular Clusters, ed. S. G. Djorgovski & G. Meylan (San Francisco, CA:ASP), 357
Talpur, Jon (1997). "A Guide to Globular Clusters". Keele University. Retrieved 2007-04-25.
Tran, H. D., Sirianni, M., Ford, H. C., et al. 2003, ApJ, 585, 750
van den Bergh, Mackey, 2004,MNRAS, 354, 713
van der Marel, Roeland, P., Cretton, N., de Zeeuw, P. Tim, Rix, Hans-Walter, 1998, AJ, 493,

613
West, M. J., Cote, P., Marzke, R. O., Jordán, A. 2004, Nature, 427, 31
Whitmore, B. C., Zhang, Q., Leitherer, C., et al. 1999, AJ, 118, 1551
Whitmore, B. C., Chandar, R., Schweizer, F., et al. 2010, AJ, 140, 75
Wirth A., Gallagher, III J. S., 1984, ApJ, 282, 85
Yale University. (2008, April 29). Ultra-dense Galaxies Found In Early Universe. ScienceDaily. Retrieved April 5, 2018 from www.sciencedaily.com/releases/2008/04/080429095054.htm

Chapter 9

Appendix

In Tables 9.1, 9.2 and 9.3 we show the result of all 81 simulations of cE. In the table you can see the characteristic of the simulations: the size of a single SC/UCD(R_{sc}), the size of the distribution or CC (R_{cc}) and the distance to the center of the galaxy of the distribution(R_{gal}). Also 3 differents random numbers are given in each set of initial parameters. And separed with a double line are the characteristics of the final object: it is possible to see the number of the SCs in the merger object(N_{merger}), the total particles in the merger object, the final effective radius($R_{\rm eff}$), the ellipticity, the velocity dispersion (σ_0) and the central surface brightness of the final object(Σ_0).

Name	Random N	R_{sc}[pc]	R_{cc}[pc]	R_{gal}[kpc]	N_{merger}	Particles	$R_{\rm eff}$[pc]	Ellipticity	σ_0[km/s]	Σ_0[mag/arcsec^2]
Sim43	-15	4	50	20	61	6047268	145.0±1.3	0.207±0.003	56.64	15.57
Sim54	-3737	4	50	20	62	6193465	131.2±2.2	0.049±0.002	55.74	15.78
Sim81	-54	4	50	20	62	6194538	118.0±3.6	0.054±0.003	57.42	15.55
Sim44	-15	4	50	60	61	5837215	150.4±1.6	0.083±0.003	55.89	15.80
Sim55	-3737	4	50	60	62	6091763	139.3±1.4	0.005±0.003	55.58	15.91
Sim82	-54	4	50	60	64	6331753	130.4±3.6	0.072±0.003	57.07	15.55
Sim40	-15	4	50	100	61	5751101	150.2±1.5	0.157±0.003	55.84	15.80
Sim56	-3737	4	50	100	63	5899974	135.3±2.1	0.022±0.004	55.65	15.91
Sim83	-54	4	50	100	64	5931195	130.4±3.3	0.055±0.003	55.01	15.57
Sim31	-15	10	50	20	63	6299876	101.8±14.0	0.081±0.002	72.75	14.99
Sim57	-3737	10	50	20	64	6399992	108.2±15.7	0.083±0.002	67.49	15.03
Sim84	-54	10	50	20	64	6399908	86.1±11.6	0.138±0.001	75.94	14.70
Sim17	-15	10	50	60	63	6265728	102.9±14.6	0.069±0.002	72.11	15.07
Sim58	-3737	10	50	60	64	6391001	109.9±16.0	0.107±0.003	67.85	14.99
Sim85	-54	10	50	60	64	6387373	87.7±12.3	0.100±0.002	74.10	14.70
Sim32	-15	10	50	100	63	6220982	102.0±14.4	0.067±0.002	73.98	15.01
Sim59	-3737	10	50	100	64	6314087	111.3±16.5	0.098±0.002	67.06	15.01
Sim86	-54	10	50	100	64	6070632	89.0±12.7	0.105±0.002	72.50	14.70
Sim20	-15	20	50	20	64	6394357	89.4±6.6	0.138±0.002	85.97	14.92
Sim60	-3737	20	50	20	64	6399974	94.6±7.7	0.132±0.002	77.87	14.91
Sim87	-54	20	50	20	64	6399989	85.8±6.6	0.012±0.002	82.92	14.90
Sim19	-15	20	50	60	64	6335047	89.1±6.4	0.149±0.003	87.14	15.00
Sim61	-3737	20	50	60	64	6389978	94.4±7.7	0.128±0.002	78.89	14.91
Sim88	-54	20	50	60	64	6395892	85.7±6.0	0.134±0.003	82.21	14.75
Sim23	-15	20	50	100	64	6298754	89.3±6.1	0.259±0.001	83.12	14.86
Sim62	-3737	20	50	100	64	6346350	94.8±7.3	0.141±0.002	79.23	14.94
Sim89	-54	20	50	100	64	6372578	85.7±5.9	0.101±0.002	82.50	14.79

Table 9.1: Table results of all 27 simulations of cE with initial R_{cc}=50 pc. The initial parameters are shown and separated with a double line are the characteristic of the final object.

Name	Random N	R_{sc}[pc]	R_{cc}[pc]	R_{gal}[kpc]	N_{merger}	Particles	$R_{\rm eff}$[pc]	Ellipticity	σ_0[km/s]	Σ_0[mag/arcsec^2]
Sim41	-15	4	100	20	62	6184345	186.5±1.7	0.153±0.002	53.02	15.93
Sim63	-3737	4	100	20	39	3896881	193.5±4.7	0.186±0.004	40.65	16.49
Sim90	-54	4	100	20	50	4997081	138.0±1.6	0.198±0.004	56.89	15.80
Sim42	-15	4	100	60	62	5922462	194.7 ±3.0	0.133±0.003	52.70	15.92
Sim64	-3737	4	100	60	33	3270680	196.3 ±5.5	0.204±0.004	39.34	16.53
Sim91	-54	4	100	60	47	4647758	133.1±1.4	0.209±0.003	56.76	15.79
Sim35	-15	4	100	100	62	5452028	195.7 ±3.5	0.366±0.002	50.00	15.97
Sim65	-3737	4	100	100	38	3578342	202.4±6.3	0.038±0.004	39.58	16.62
Sim92	-54	4	100	100	50	4720395	138.0±1.7	0.233±0.005	58.11	15.82
Sim38	-15	10	100	20	64	6400000	138.7±26.4	0.251±0.003	70.98	14.98
Sim66	-3737	10	100	20	64	6400000	131.0±1.7	0.139±0.002	61.93	15.25
Sim93	-54	10	100	20	64	6400000	88.8±0.7	0.084±0.002	71.47	14.91
Sim39	-15	10	100	60	64	6394826	129.7±19.7	0.311±0.004	70.30	15.17
Sim67	-3737	10	100	60	64	6399858	135.9±1.8	0.124±0.002	62.44	15.29
Sim94	-54	10	100	60	64	6397470	89.3±0.7	0.085±0.003	69.68	14.94
Sim30	-15	10	100	100	64	6367372	128.8 ±19.1	0.100±0.002	69.71	15.21
Sim68	-3737	10	100	100	64	6389248	137.3±2.1	0.153±0.002	58.84	15.25
Sim95	-54	10	100	100	64	6320067	89.6±0.7	0.062±0.002	69.61	14.97
Sim36	-15	20	100	20	64	6399952	119.5±10.7	0.398±0.002	73.53	15.26
Sim69	-3737	20	100	20	64	6400000	120.7±0.9	0.085±0.002	65.62	15.26
Sim96	-54	20	100	20	64	6400000	105.7±9.4	0.079±0.002	76.04	15.11
Sim37	-15	20	100	60	64	6389379	117.5±9.2	0.303±0.001	73.30	15.30
Sim70	-3737	20	100	60	64	6399891	122.0±0.8	0.043±0.002	65.78	15.35
Sim97	-54	20	100	60	64	6399962	106.1±9.2	0.215±0.003	73.99	14.99
Sim25	-15	20	100	100	64	6382116	118.0 ±9.6	0.081±0.002	73.38	15.31
Sim71	-3737	20	100	100	64	6388213	121.7±0.8	0.006±0.002	65.56	15.37
Sim98	-54	20	100	100	64	6389549	105.8±9.2	0.184±0.002	74.32	15.04

Table 9.2: Same as 9.1 but with an initial R_{cc}=100 pc.

Name	Random N	R_{sc}[pc]	R_{cc}[pc]	R_{gal}[kpc]	N_{merger}	Particles	$R_{\rm eff}$[pc]	Ellipticity	σ_0[km/s]	Σ_0[mag/arcsec^2]
Sim51	-15	4	200	20	34	3390263	276.3±8.1	0.301±0.004	28.69	17.01
Sim72	-3737	4	200	20	11	1099993	217.8±15.0	0.184±0.007	17.87	17.51
Sim99	-54	4	200	20	33	3299287	233.0±5.2	0.113±0.004	34.82	17.28
Sim52	-15	4	200	60	34	3122050	298.9±12.5	0.117±0.006	27.94	17.23
Sim73	-3737	4	200	60	11	1090881	214.9±10.1	0.145±0.006	18.54	17.48
Sim100	-54	4	200	60	33	3254492	239.4±6.6	0.270±0.004	32.97	17.01
Sim53	-15	4	200	100	33	2796717	284.9±8.9	0.141±0.006	27.93	17.23
Sim74	-3737	4	200	100	11	1020625	241.2±14.8	0.199±0.006	18.37	17.43
Sim101	-54	4	200	100	31	2868578	246.0±7.1	0.200±0.005	32.37	17.00
Sim45	-15	10	200	20	64	6400000	187.2±3.5	0.114±0.003	53.73	15.48
Sim75	-3737	10	200	20	64	6400000	264.2±1.9	0.115±0.004	48.07	15.64
Sim102	-54	10	200	20	64	6400000	140.2±2.1	0.159±0.002	56.89	15.30
Sim46	-15	10	200	60	64	6394414	183.2±1.9	0.163±0.002	52.31	15.49
Sim76	-3737	10	200	60	64	6399999	273.3±47.7	0.113±0.003	45.82	15.62
Sim103	-54	10	200	60	64	6399979	140.5±2.0	0.143±0.002	57.58	15.44
Sim47	-15	10	200	100	64	6363237	191.1±2.9	0.135±0.004	51.14	15.42
Sim77	-3737	10	200	100	64	6378933	271.6±5.2	0.117±0.005	46.90	15.58
Sim104	-54	10	200	100	64	6365416	141.7±2.3	0.166±0.003	56.10	15.31
Sim48	-15	20	200	20	64	6400000	177.7±1.0	0.444±0.005	57.67	15.97
Sim78	-3737	20	200	20	64	6400000	247.8±8.0	0.275±0.006	48.26	16.11
Sim105	-54	20	200	20	64	6400000	152.6±1.3	0.235±0.002	59.29	15.60
Sim49	-15	20	200	60	64	6398500	176.6±0.7	0.381±0.005	56.60	16.06
Sim79	-3737	20	200	60	64	6400000	241.1±10.3	0.227±0.004	47.99	16.18
Sim106	-54	20	200	60	64	6400000	154.8±1.4	0.124±0.002	58.71	15.73
Sim50	-15	20	200	100	64	6388283	179.3±0.8	0.361±0.006	55.07	15.97
Sim80	-3737	20	200	100	64	6397551	237.4±8.7	0.145±0.003	47.92	16.24
Sim107	-54	20	200	100	64	6381942	154.9±1.3	0.110±0.002	58.77	15.74

Table 9.3: Same as 9.1 but with an initial R_{cc}=200 pc.